

The Alfvén Transition Zone observed by the Parker Solar Probe in Young Solar Wind – Global Properties and Model Comparisons

Rohit Chhiber

University of Delaware & NASA Goddard Space Flight Center

Collaborators: Francesco Pecora, Arcadi Usmanov, William Matthaeus, Melvyn Goldstein, Sohom Roy, Jiaming Wang, David Ruffolo, Panisara Thepthong

PUNCH 5 Science Meeting
20th Jun 2024, Boulder, USA

Solar corona vs solar wind – where is the boundary?

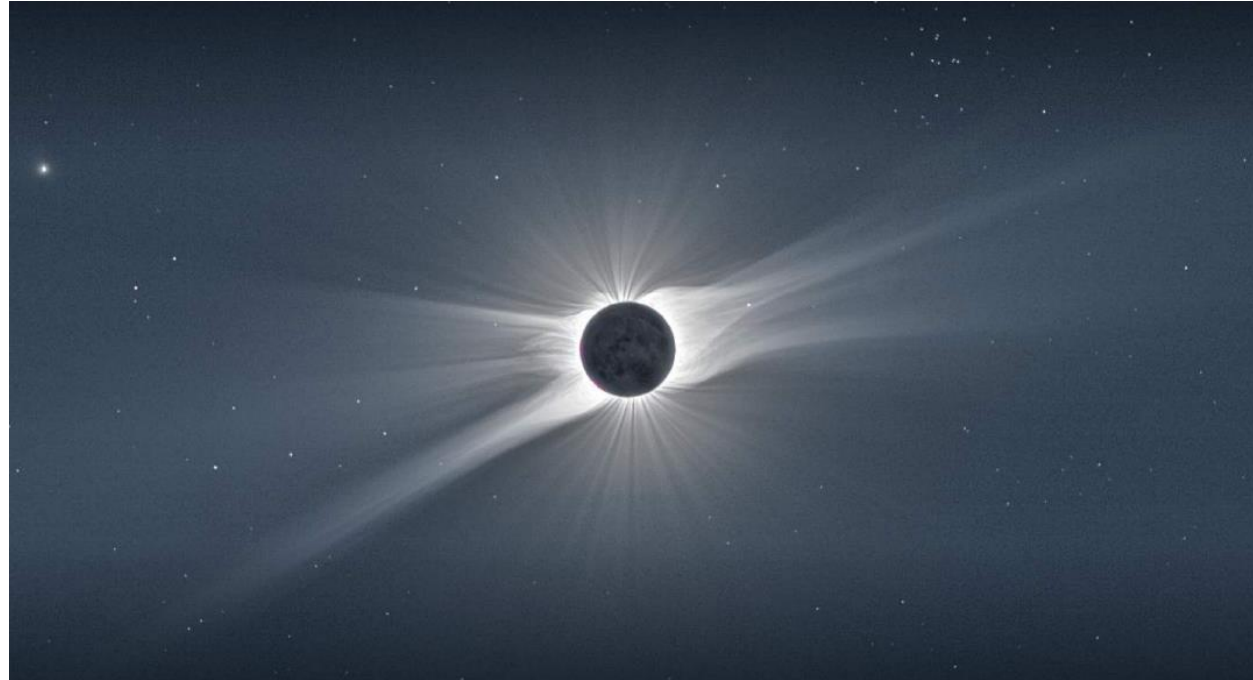


Image credit: Dr. Steve Cranmer

Critical points/surfaces -

- Flow becomes supersonic at the **sonic surface**
- Super-Alfvenic at **Alfven surface**
- $\beta = 1$ surface; magnetosonic surface
- **PUNCH Science WG1C: What are the evolving physical processes of the Alfven surface?**

Outline

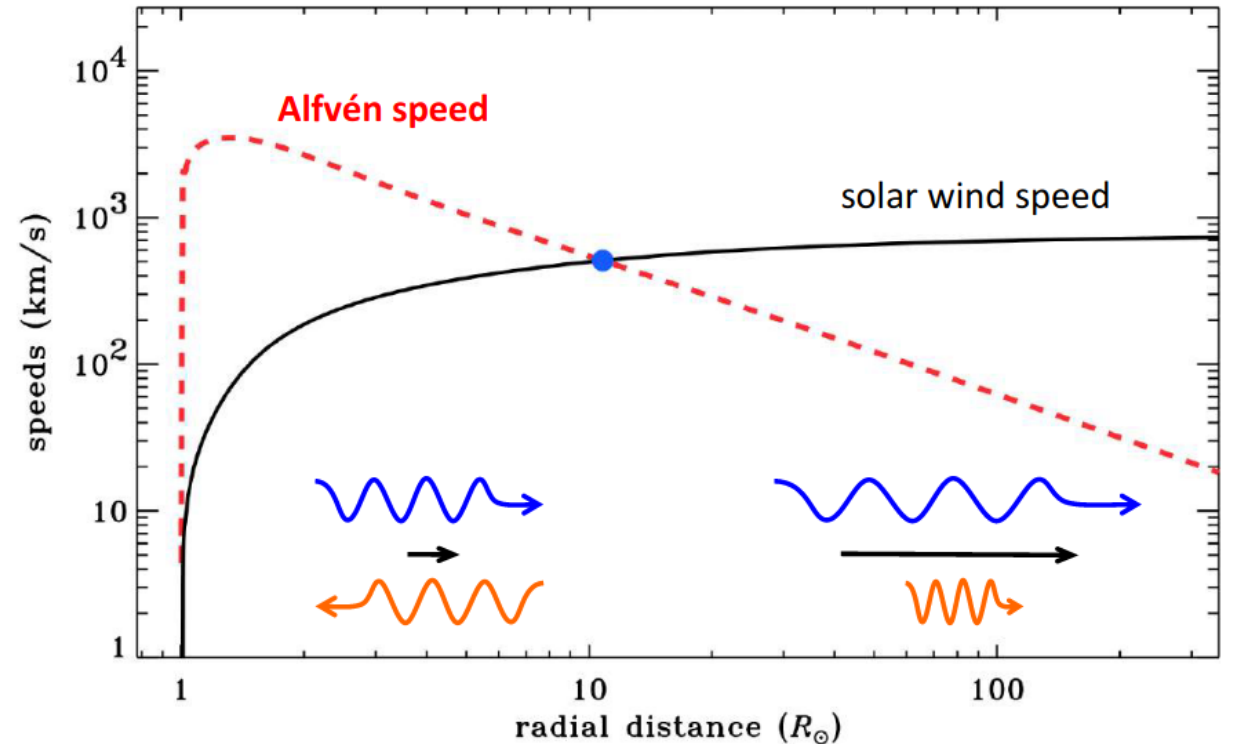
- Introduction and overview of Alfvén surface
- Some global properties – PSP vs Model
- Sunward and anti-Sunward Alfvén modes around Alfvén surface

The Alfvén "radius"

r_A is distance where $U > V_A$, where

$$V_A = \frac{B}{\sqrt{4\pi\rho}}$$

- Below r_A , information (waves) can propagate both Sunward & outward.
Above r_A , the solar wind drags out both inward & outward modes
- Strong transfer of angular momentum from Sun to wind below r_A ; Below r_A , magnetic field maintains \sim rigid rotation with Sun (Weber & Davis 1967)
- In-situ dynamics like switchback formation and flocculation may "turn on" above r_A (DeForest+ 2016; Ruffolo+ 2020; Pecora+ 2022)

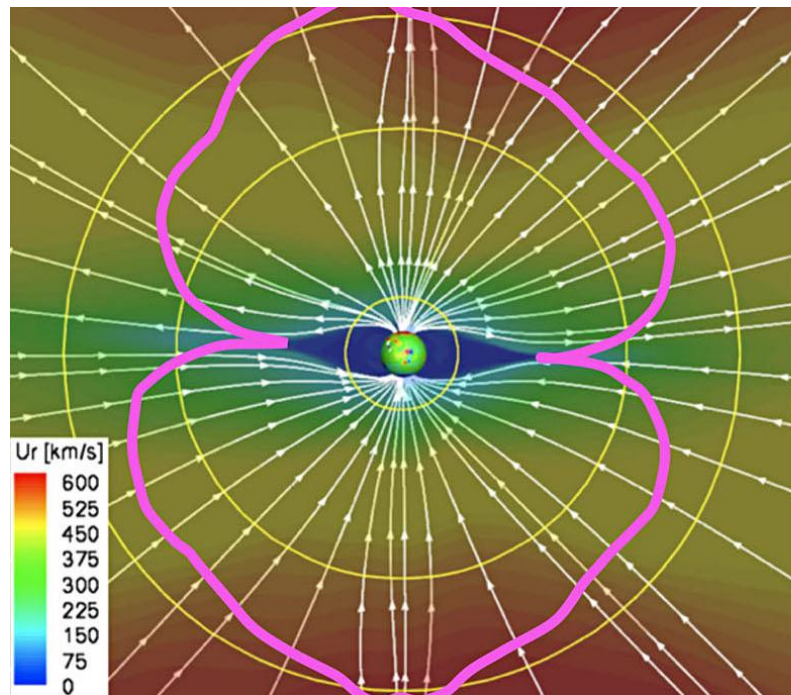


Credit: Dr. Steve Cranmer

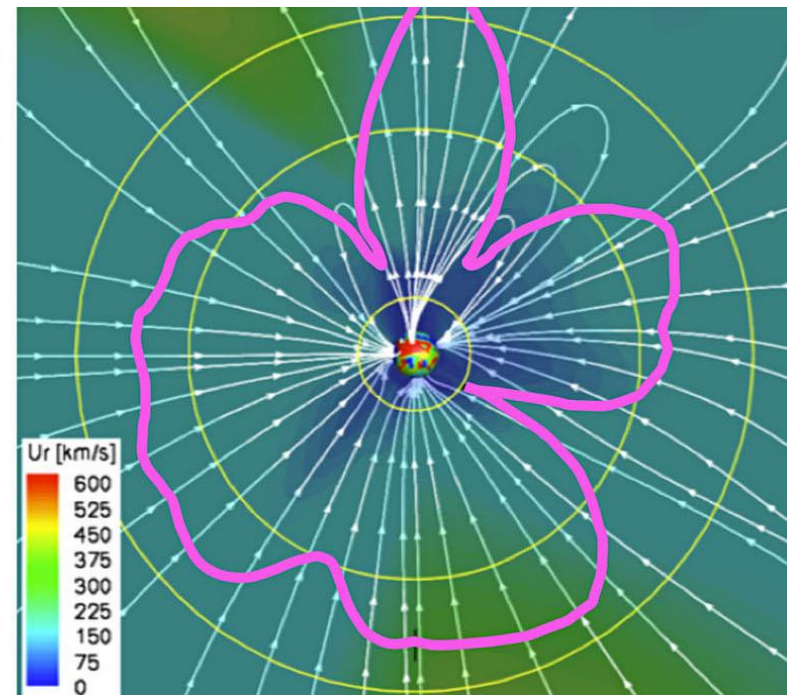
Alfven surface in 3D MHD simulations of global solar wind

Large-scale variability – solar-source related; solar activity effects

Solar min



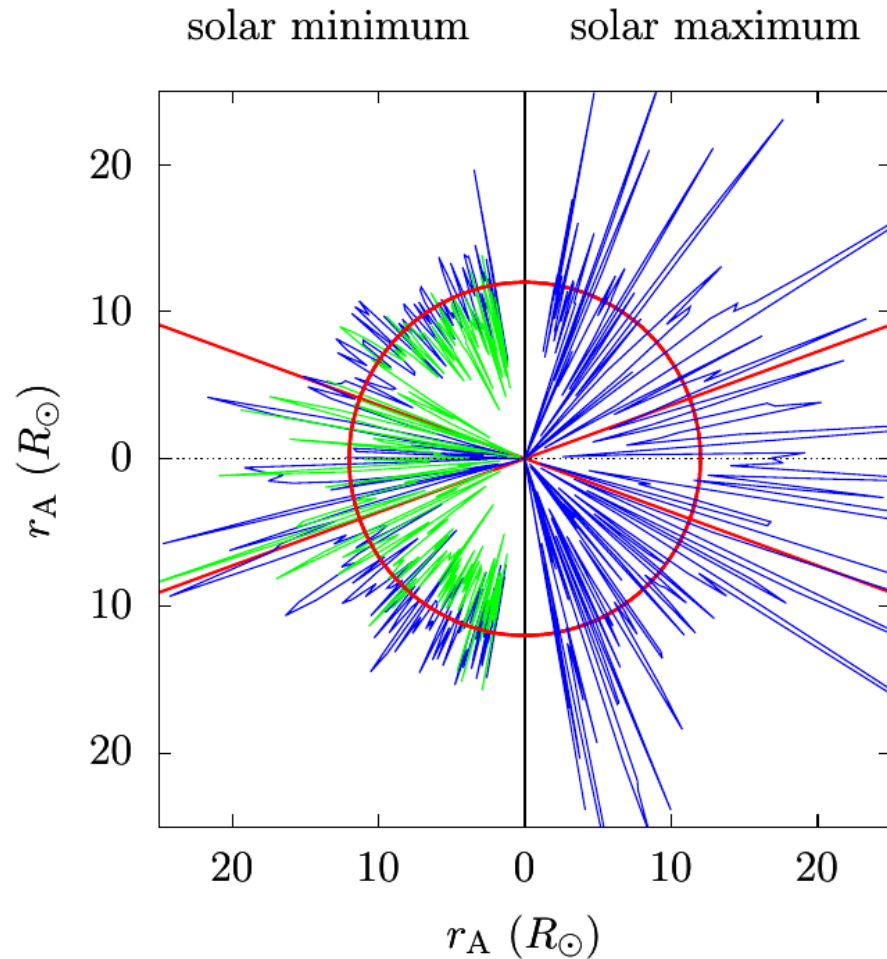
Solar max



Meridional planes (Cohen 2015; PUNCH website)

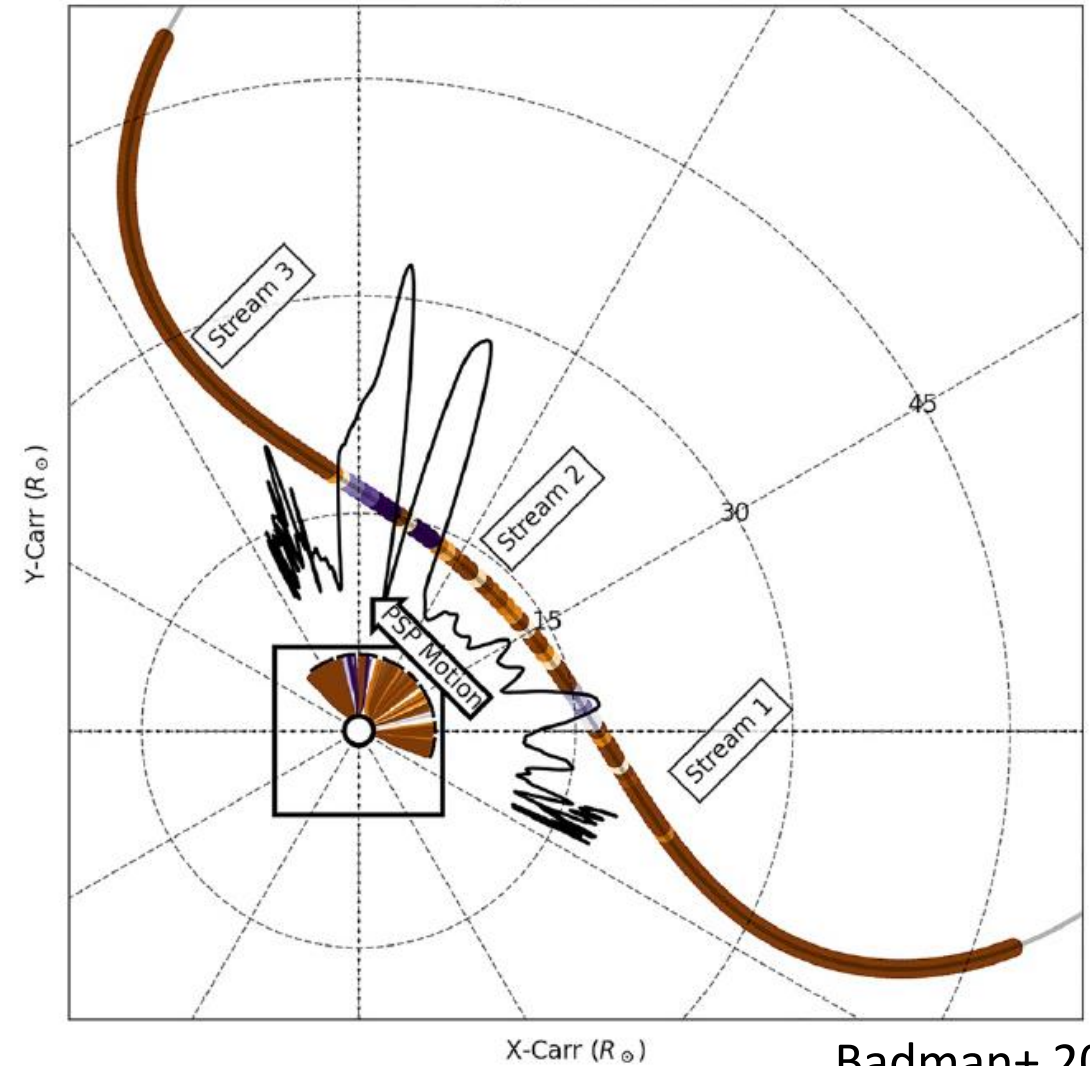
Corrugated Alfvén surface - Recent in situ observations

Verscharen+ 2021; *Ulysses*



Variability in heliolatitude

Carrington Coordinates



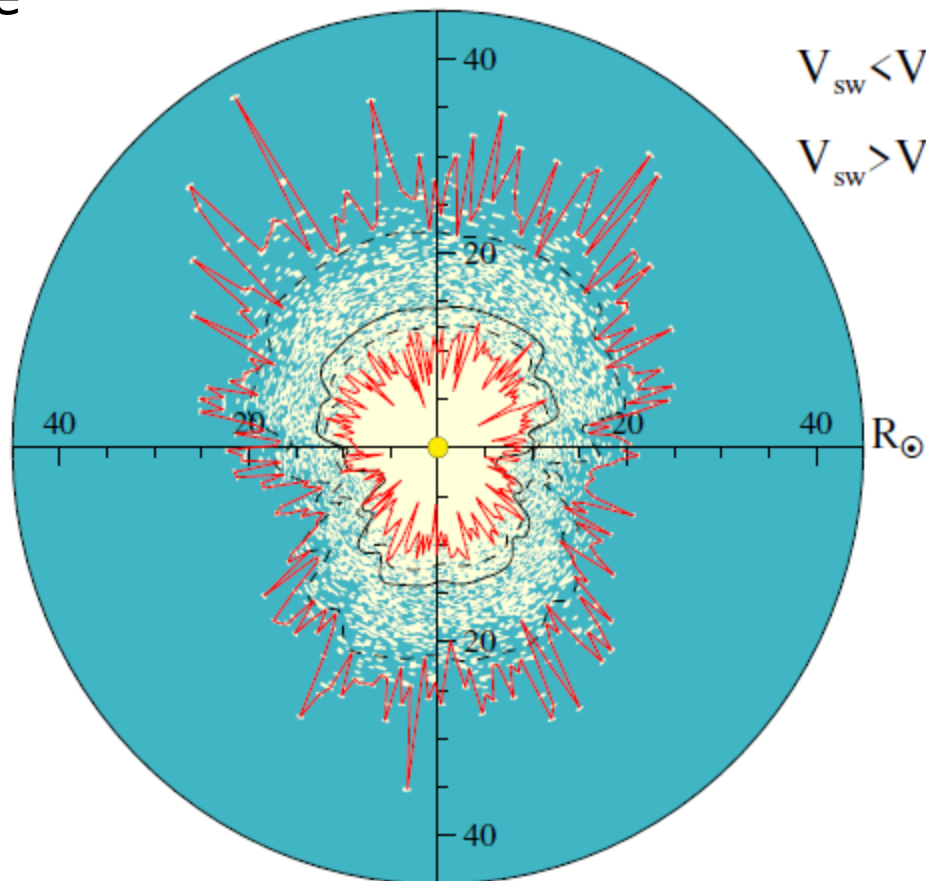
Badman+ 2023; *PSP*

Variability in heliolongitude

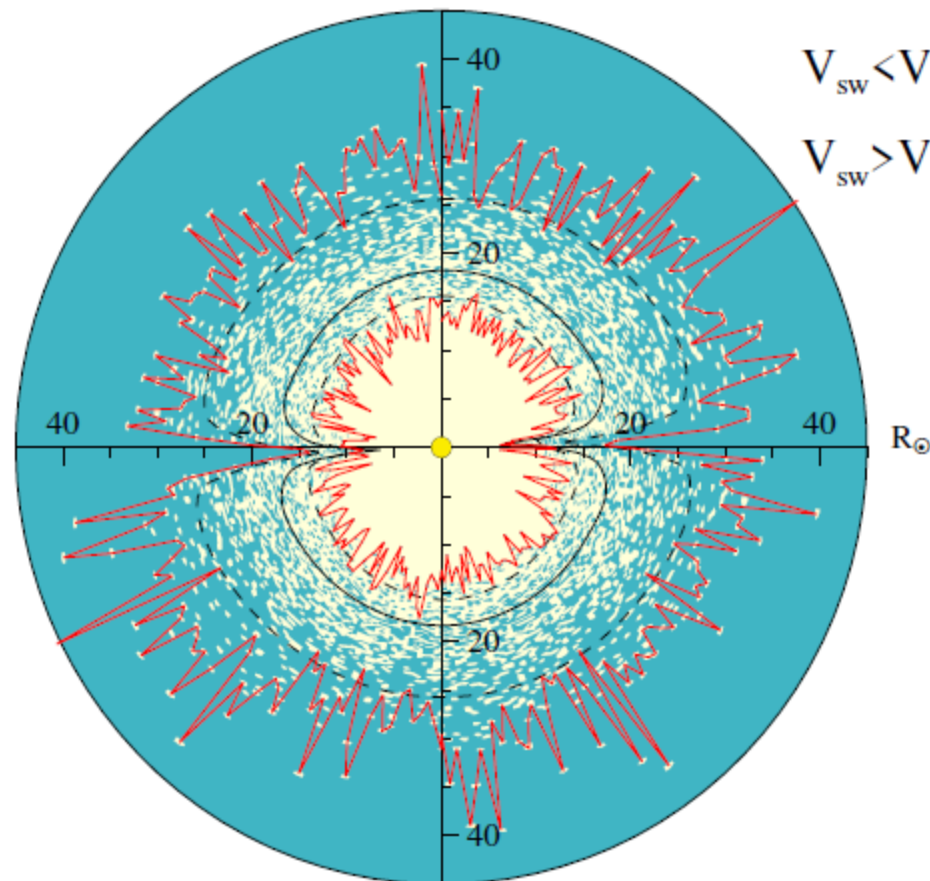
Fragmented Alfven zone from global model + turbulence

Solar equatorial plane

Meridional plane



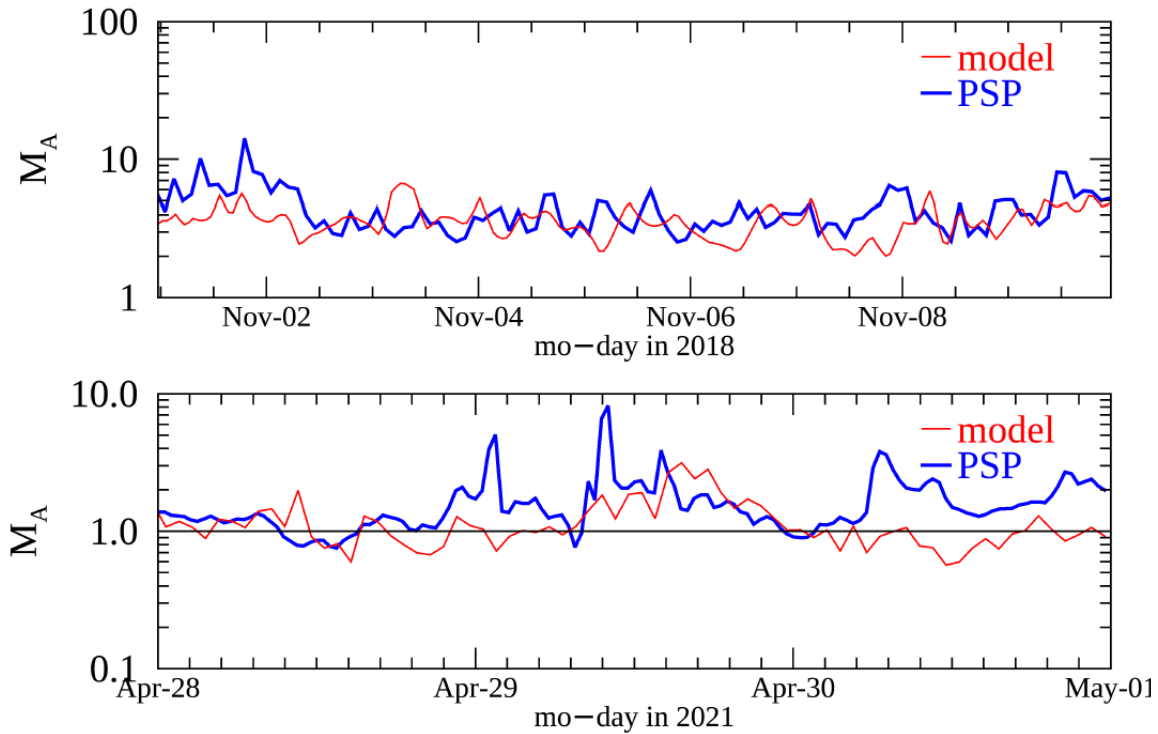
$V_{sw} < V_A$
 $V_{sw} > V_A$



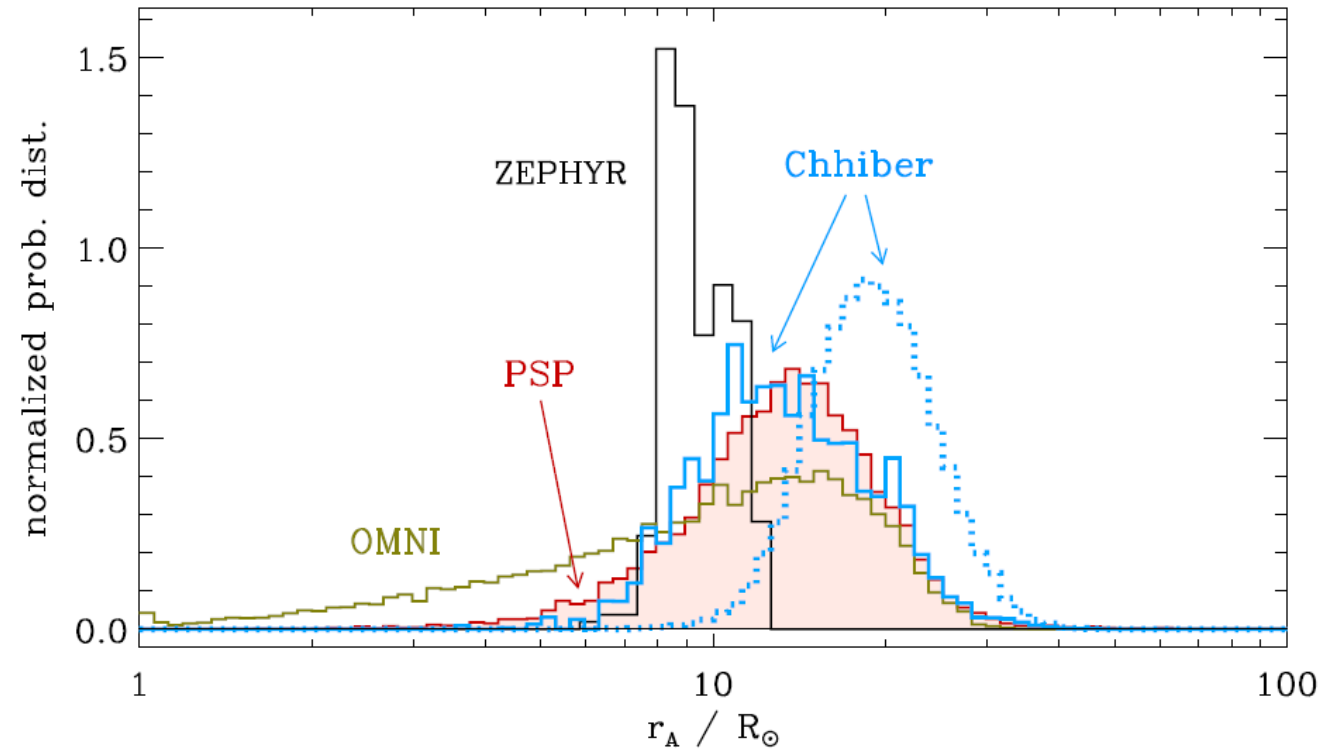
$V_{sw} < V_A$
 $V_{sw} > V_A$

Comparison with PSP observations

Virtual PSP trajectory along sim driven by magnetograms corresponding to PSP E1 and E8

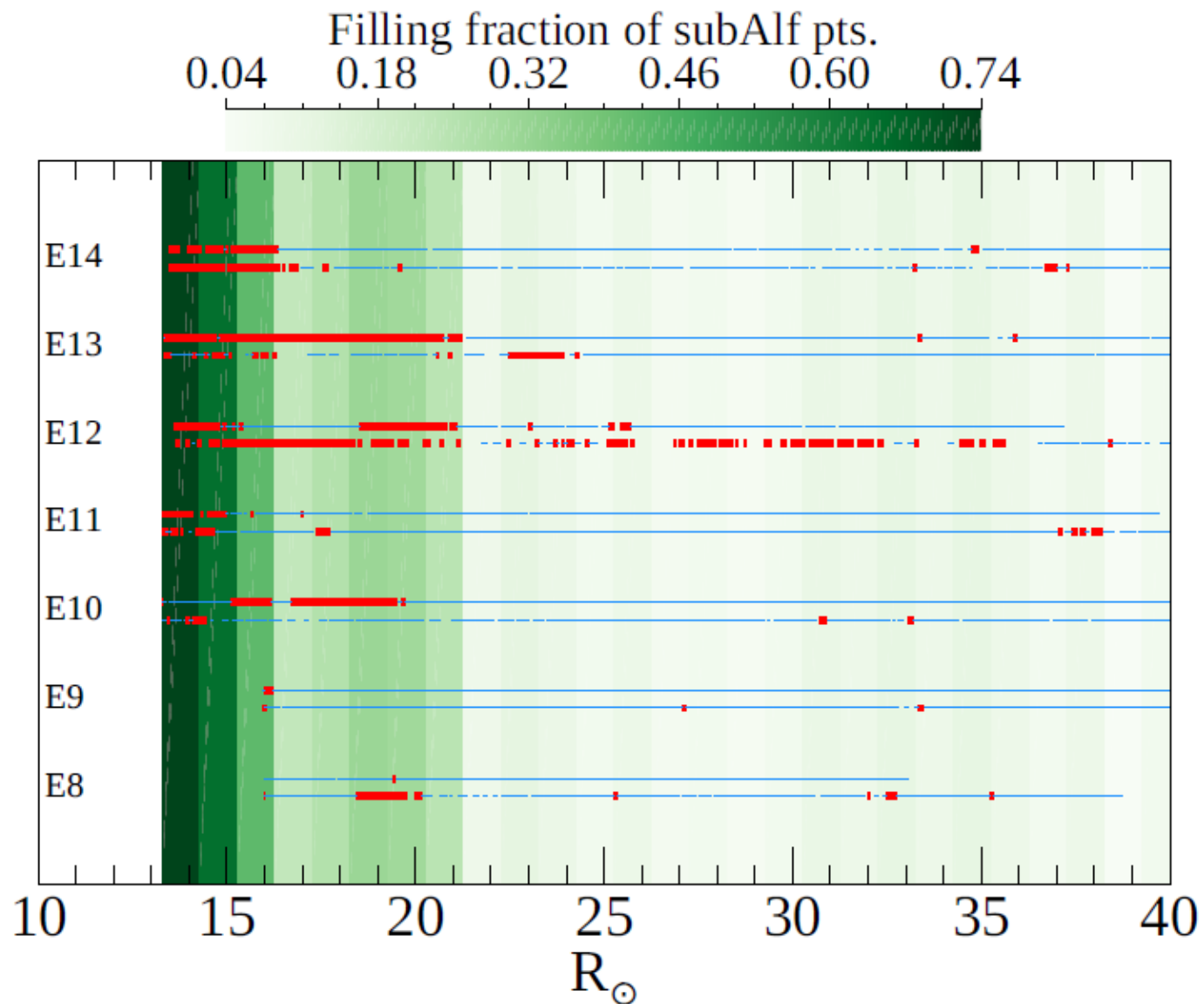
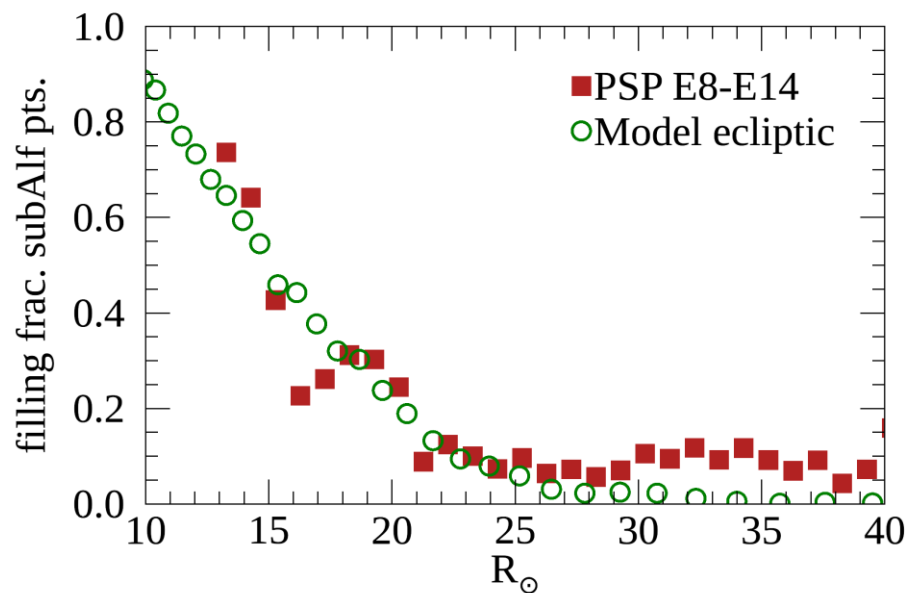


Probability of Alfvénic transition as a function of helioradius

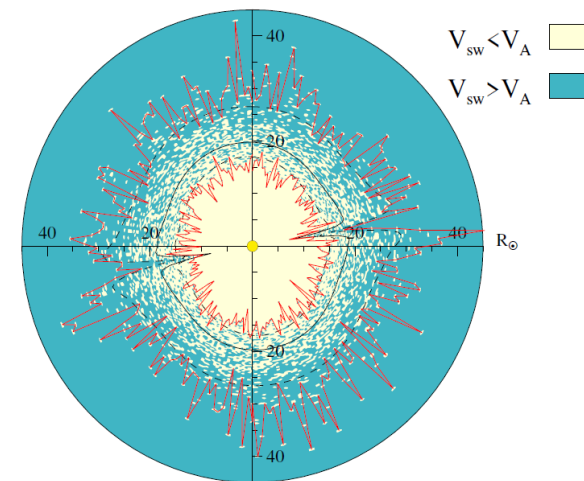
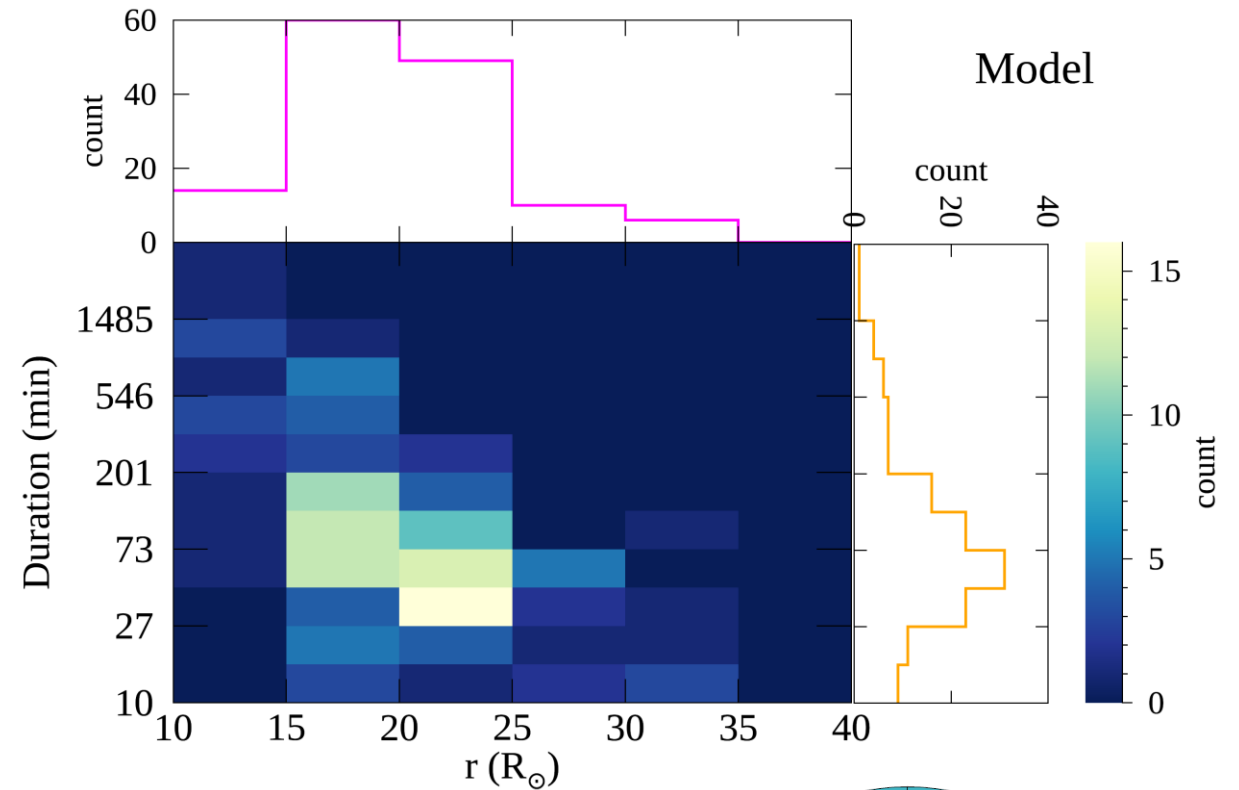
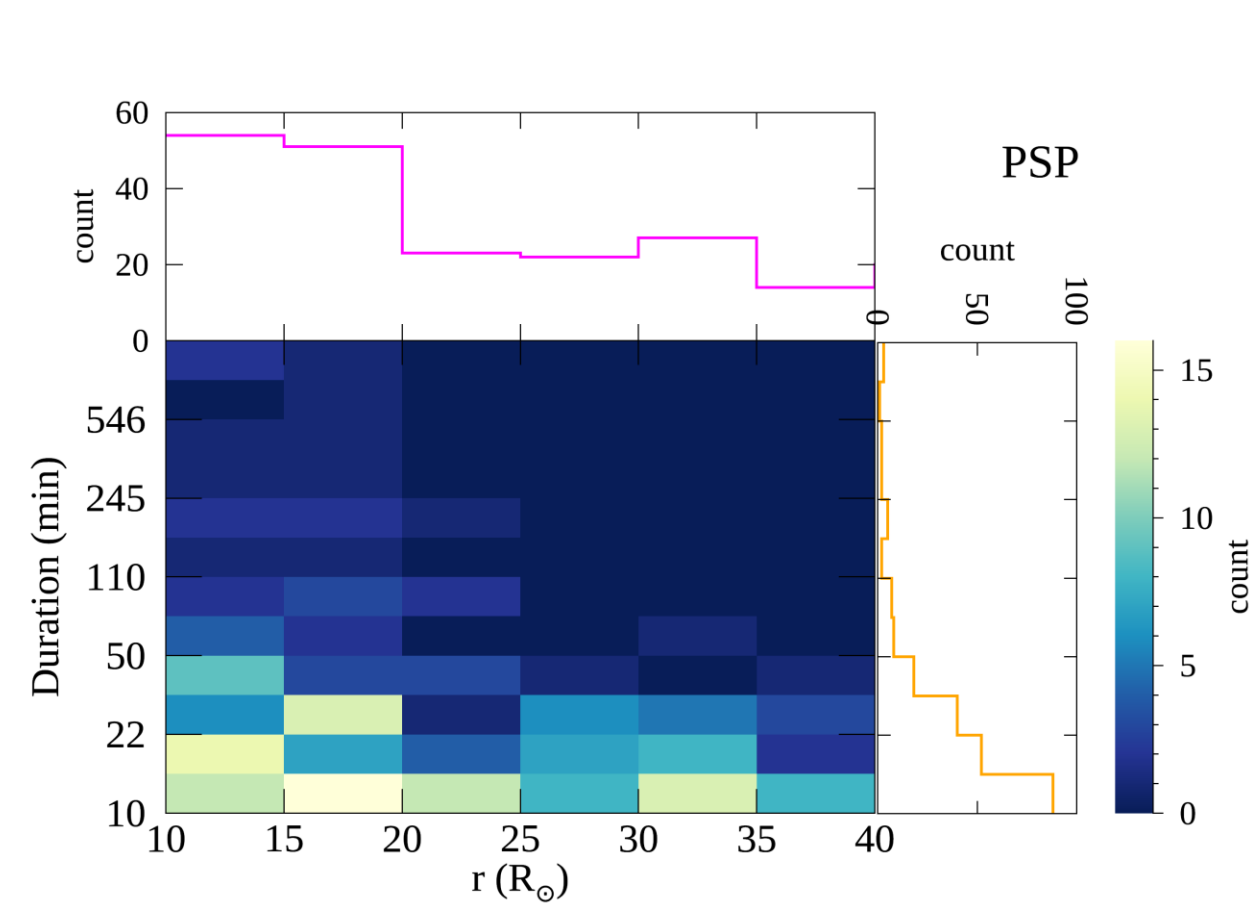


Global properties of Alfven zone – PSP and Model

- PSP data E 8 – 14
- Data resampled to 1-min cadence
- Identified subAlfvenic periods longer than 10 min duration

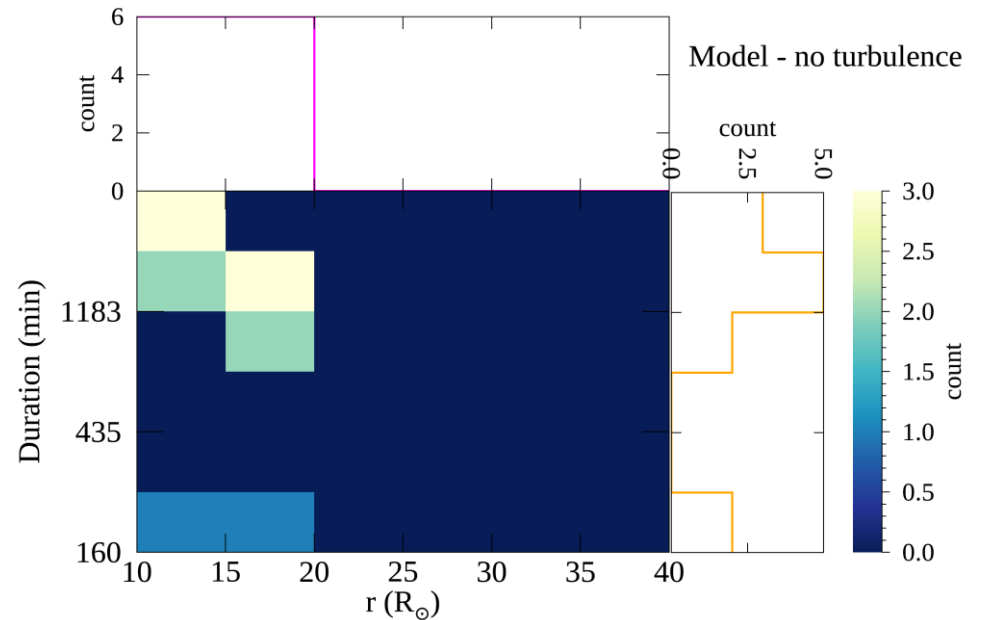
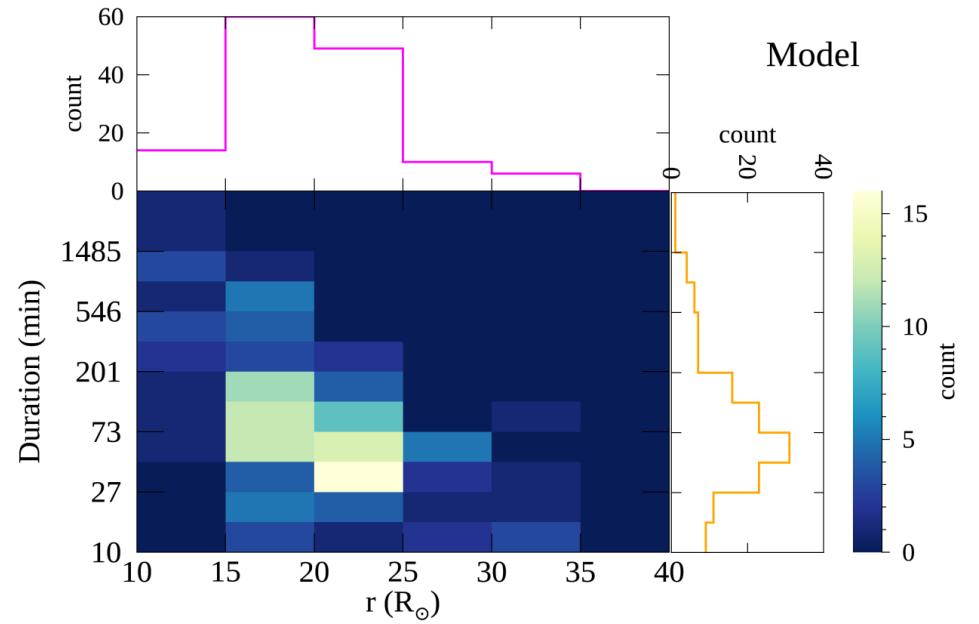
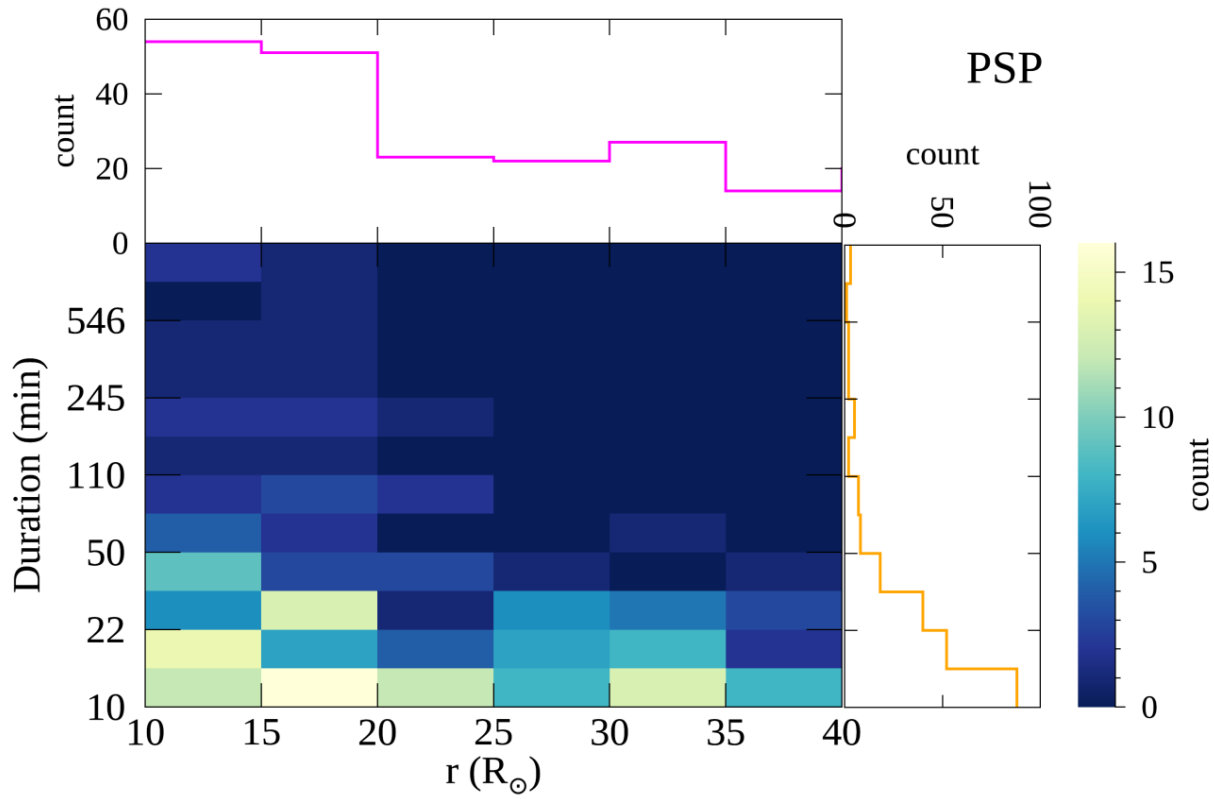


Joint distributions of subAlfvenic-interval duration and heliodistance

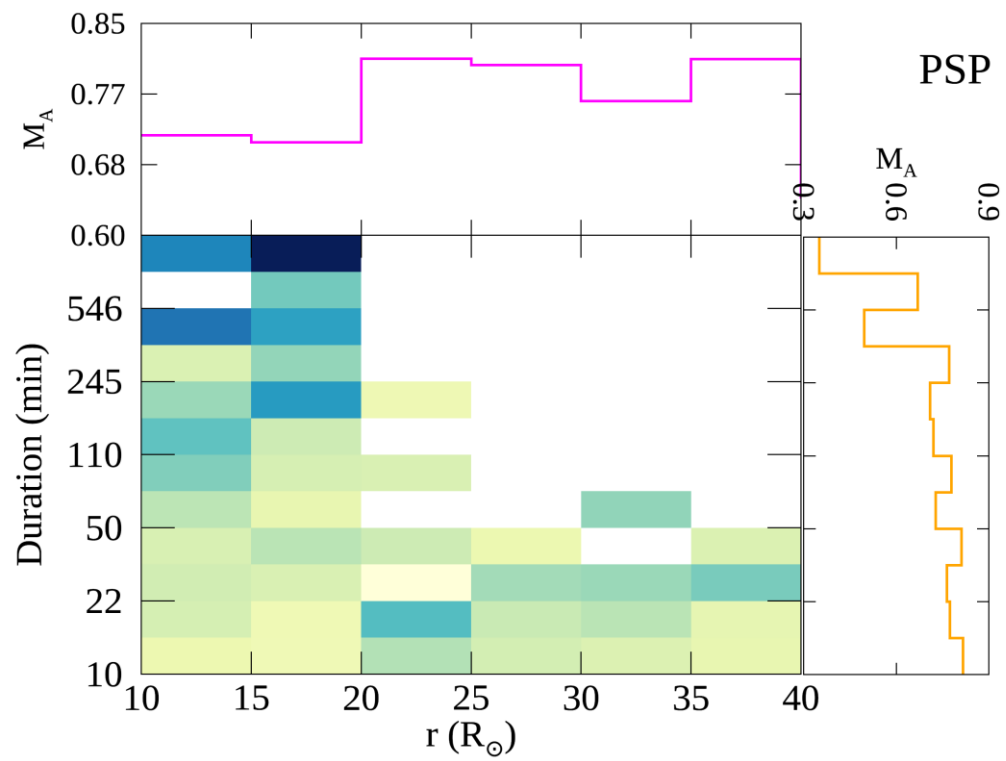


Chhiber+ 2022 prediction on Alfvén zone – both frequency and duration/size of subAlfvénic intervals will increase approaching Sun

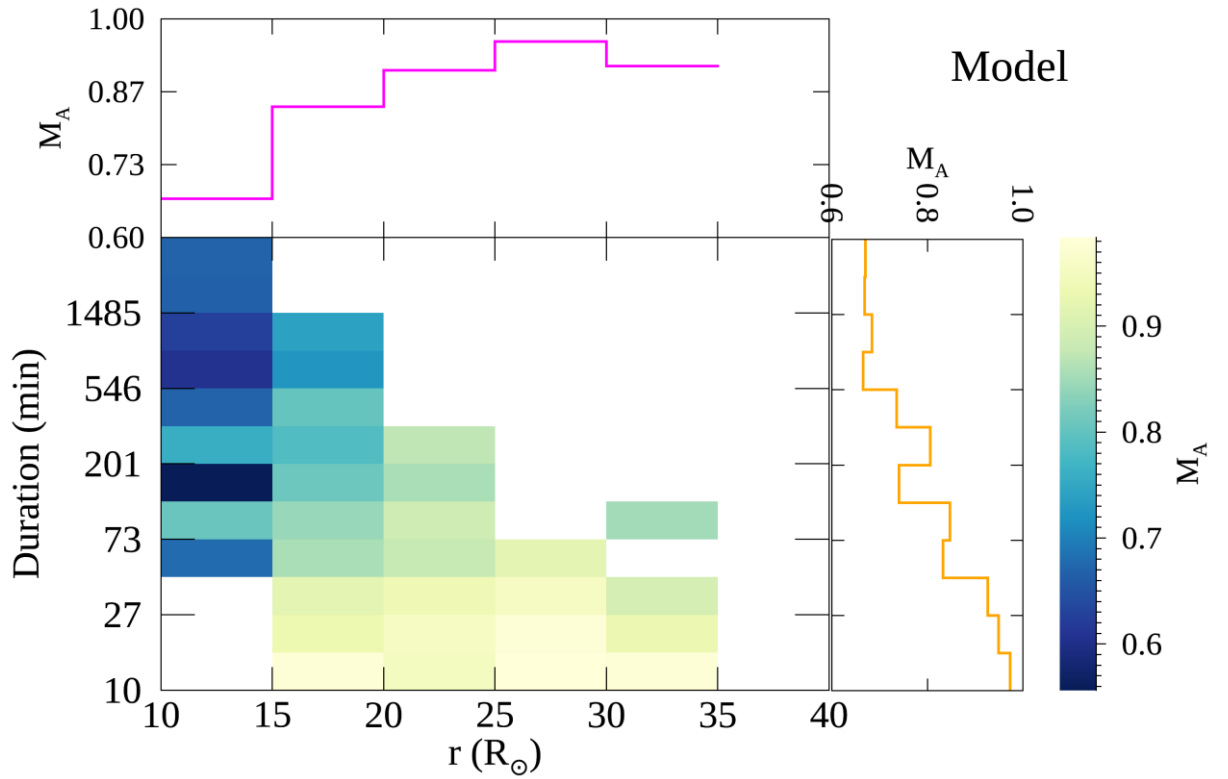
Joint distributions of subAlfvénic-interval duration and heliodistance



M_A of subAlfvenic intervals



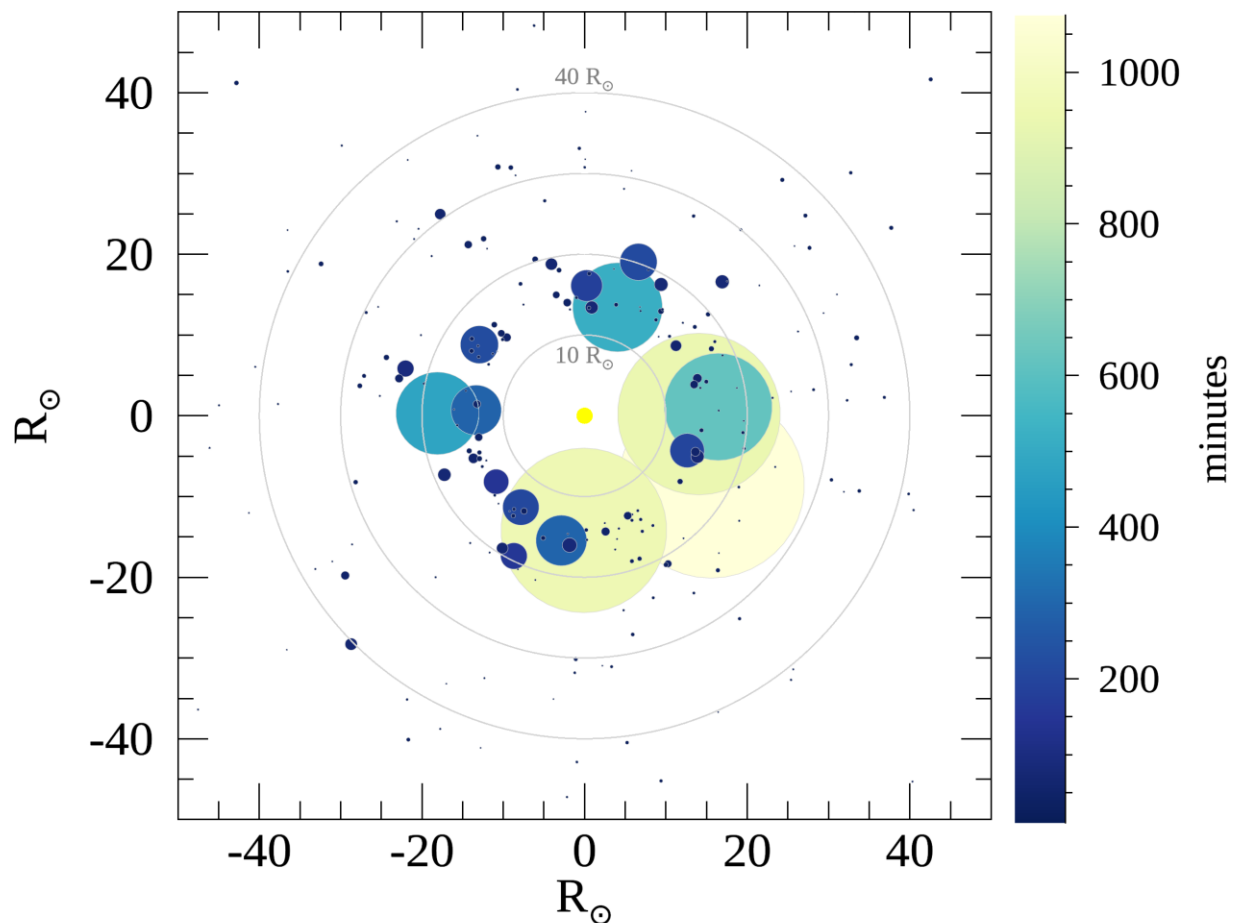
PSP



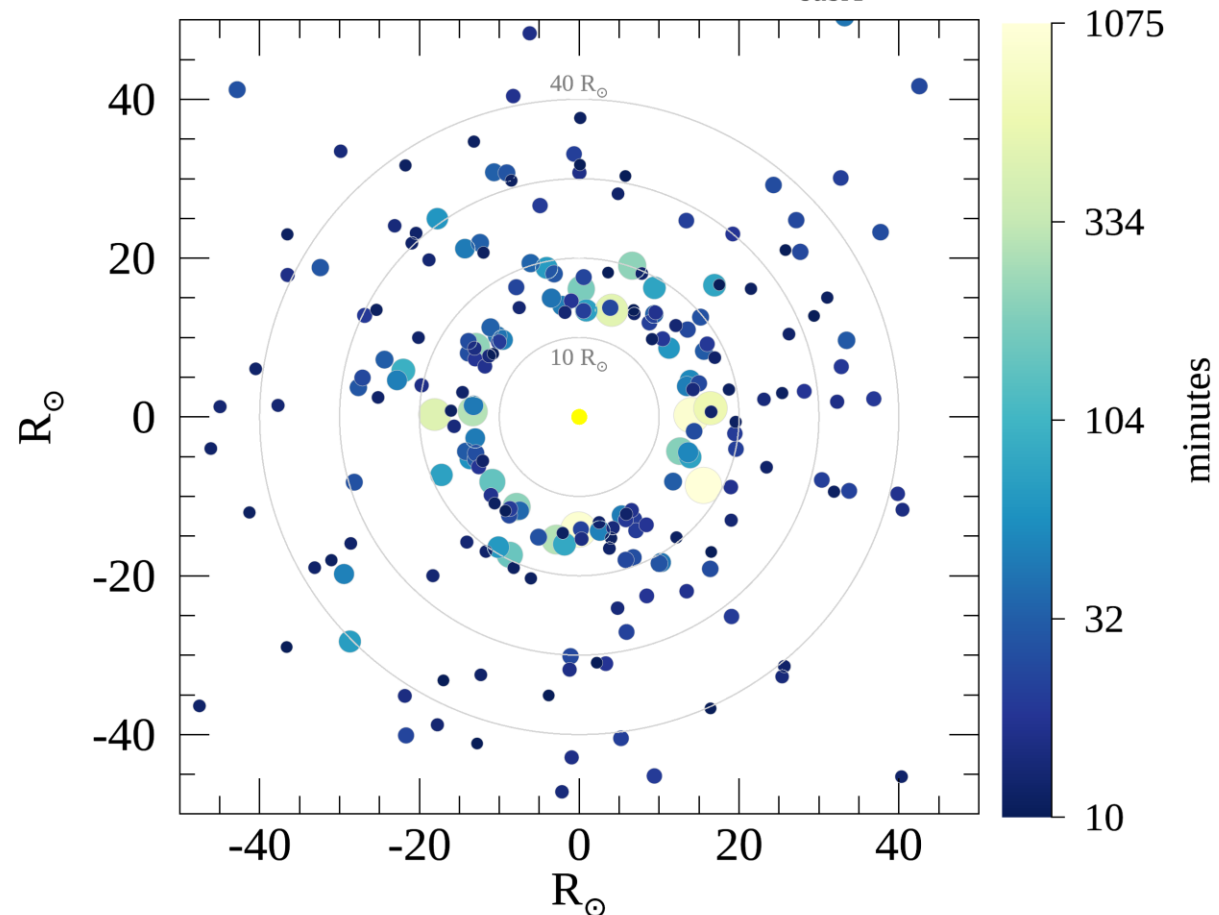
Model

“Bubble plots” of subAlfvenic interval duration

PSP E8–E14. Duration_{subA}



PSP E8–E14. ln Duration_{subA}



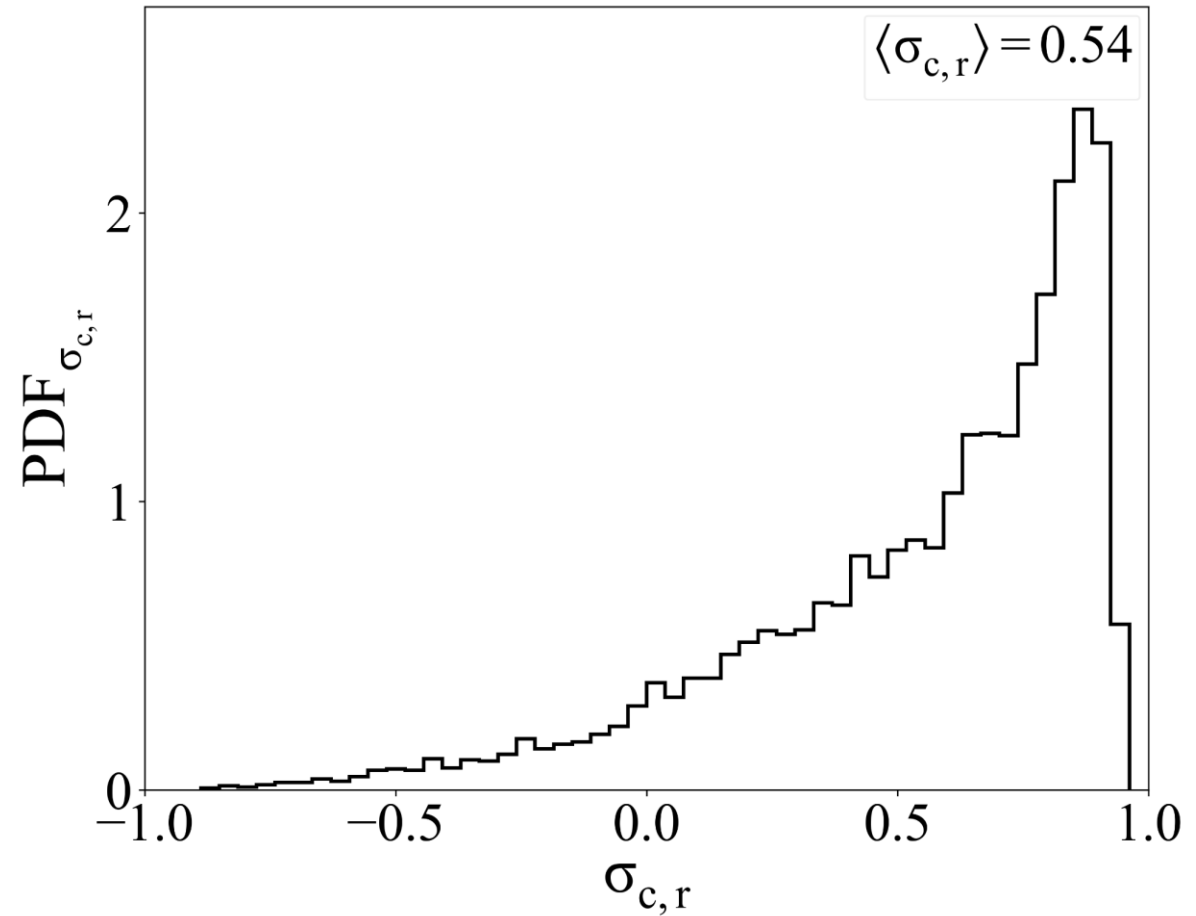
- Heliolongitude of intervals randomized
- Circle Diameter represents [*left:*] interval duration [*right:*] log (duration)
- Colorbar shows interval duration

Sunward-propagating Alfvénic signals

- Sunward propagation of Alfvénic signals indicates sub-Alfvénic solar wind flow
- Feature tracking has been used with STEREO data to infer a location for the Alfvén surface (DeForest+ 2014)
- Normalized cross helicity: $\sigma_c \equiv 2\langle \mathbf{v} \cdot \mathbf{b} \rangle / Z^2$, where $Z^2 \equiv \langle v^2 + b^2 \rangle$. Indicates correlation of velocity and magnetic fluctuations
- When $B_r > 0$ then $\sigma_c < 0$ indicates “outward” propagation of Alfvén wave; when $B_r < 0$ then $\sigma_c > 0$ is outward
- Sector rectification: when $B_r > 0$ then $\sigma_c \rightarrow -\sigma_c$. Then positive σ_c always indicates outward propagation

Sector rectified cross helicity from ten years of ACE data (1 AU)

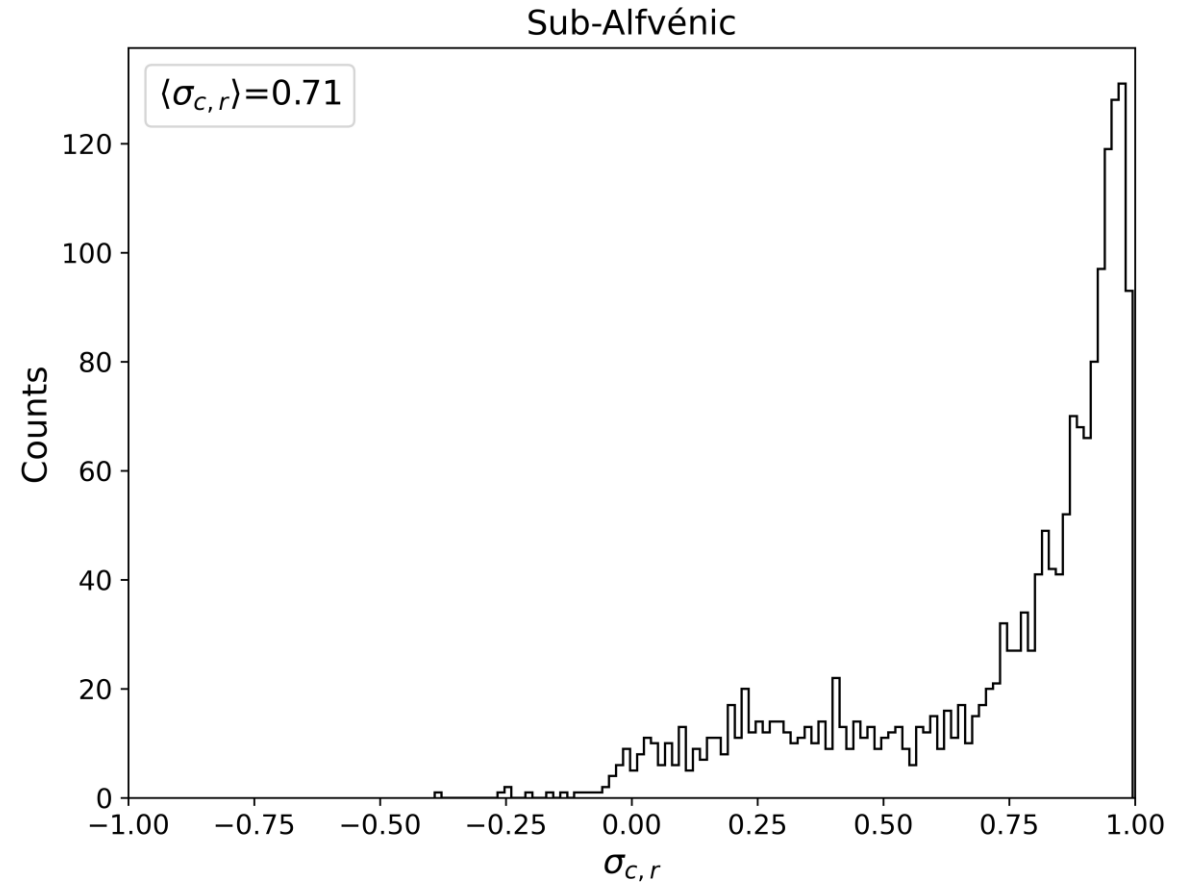
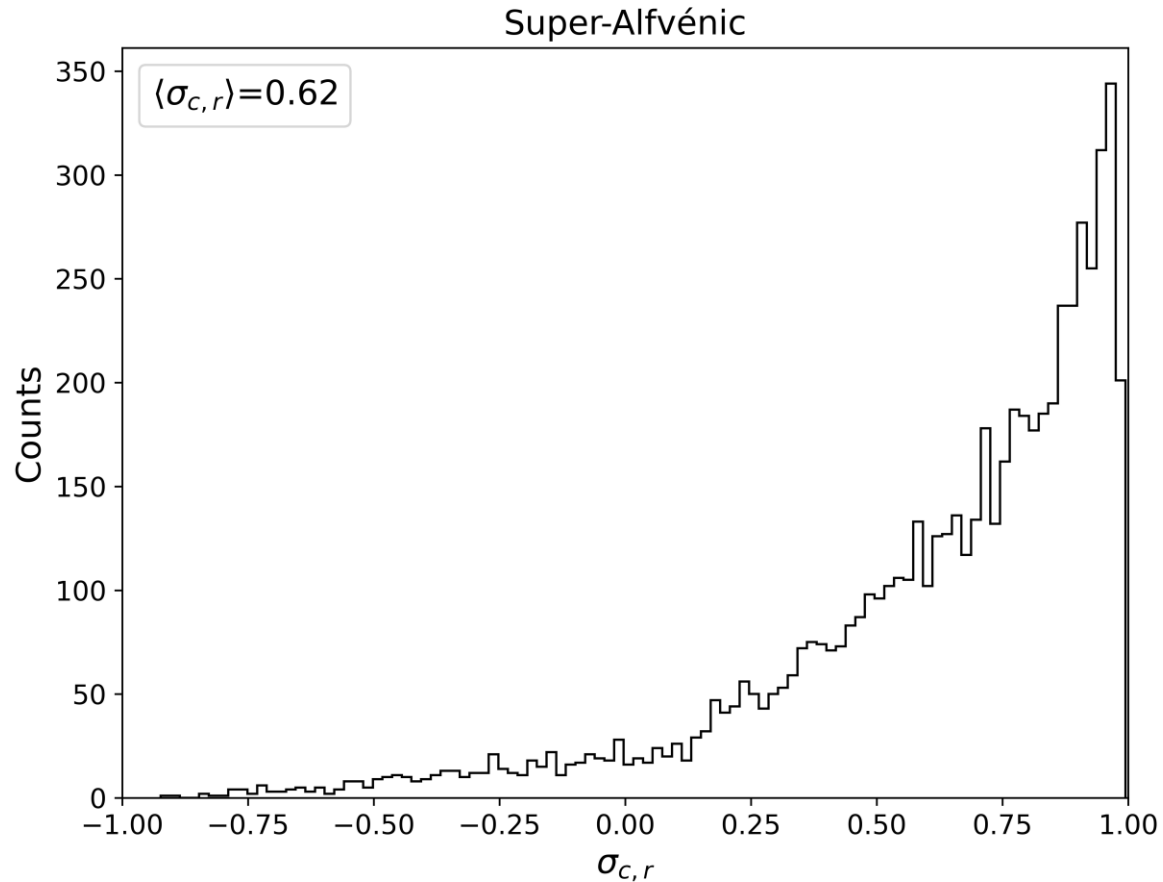
- $\sigma_c = \frac{Z_+^2 - Z_-^2}{Z_+^2 + Z_-^2}$, where Z_{\pm} are strengths of outward/inward Alfvén modes
- Figure shows PDF based on several thousand 12-hr intervals



Credit: Victoria Wang

Sector rectified cross helicity from PSP encounters (13-30 R_{\odot})

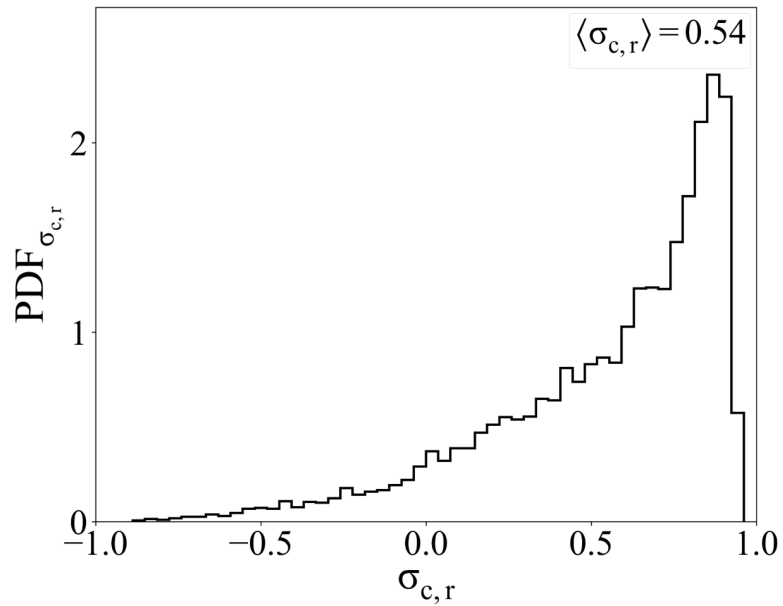
(Preliminary)



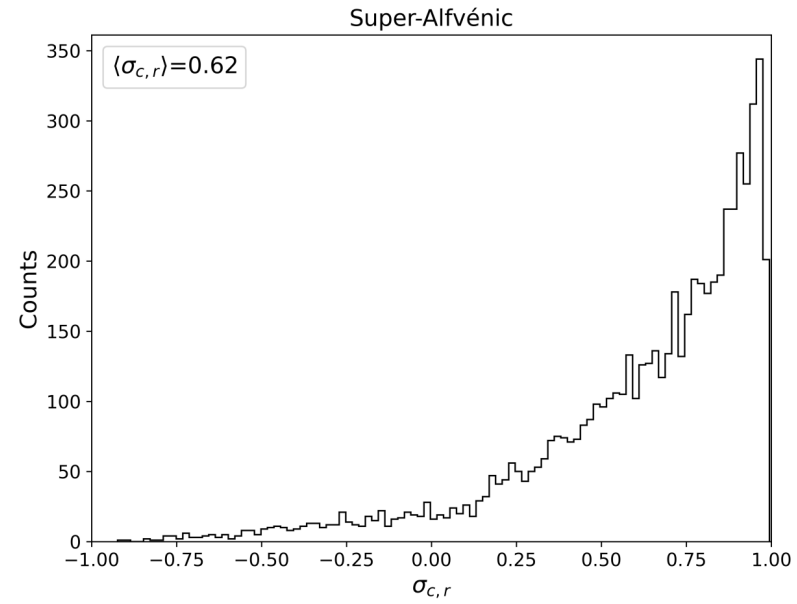
Credit: Sohom Roy

- 10-min intervals
- Almost no subAlfvénic intervals with dominant Sunward propagation

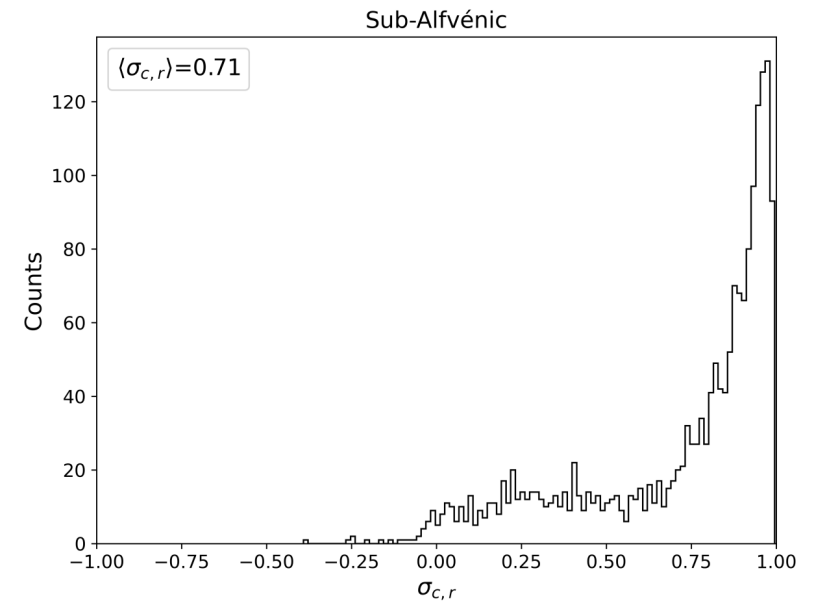
Sector rectified cross helicity in the inner heliosphere (Preliminary)



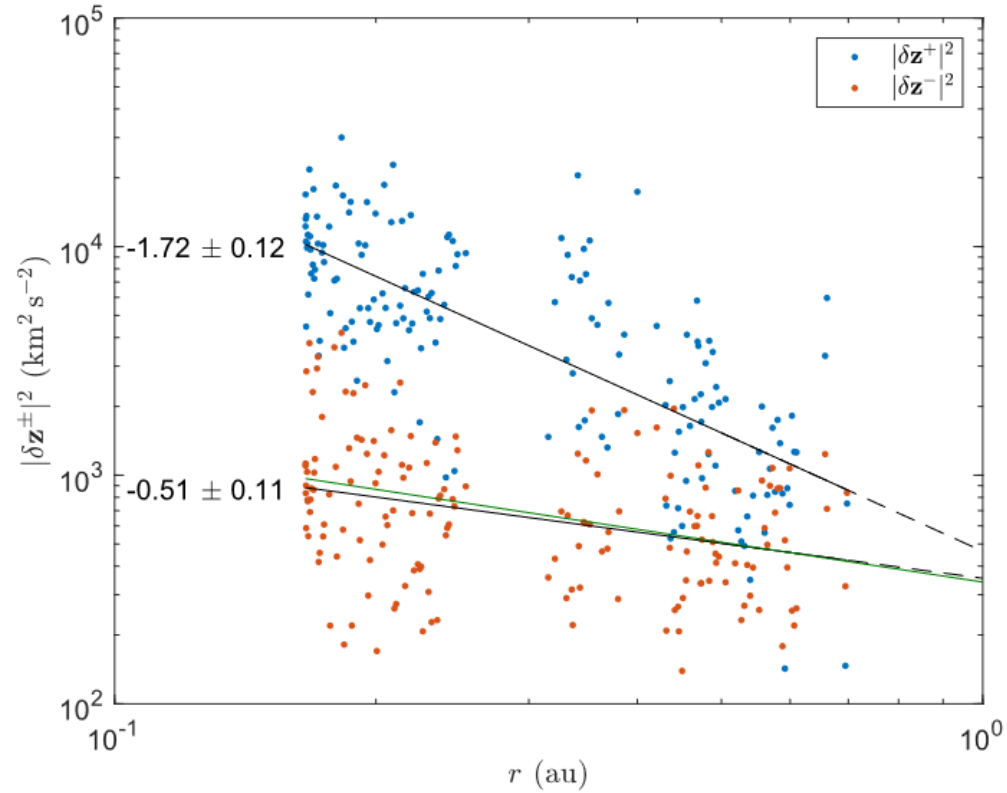
1 AU



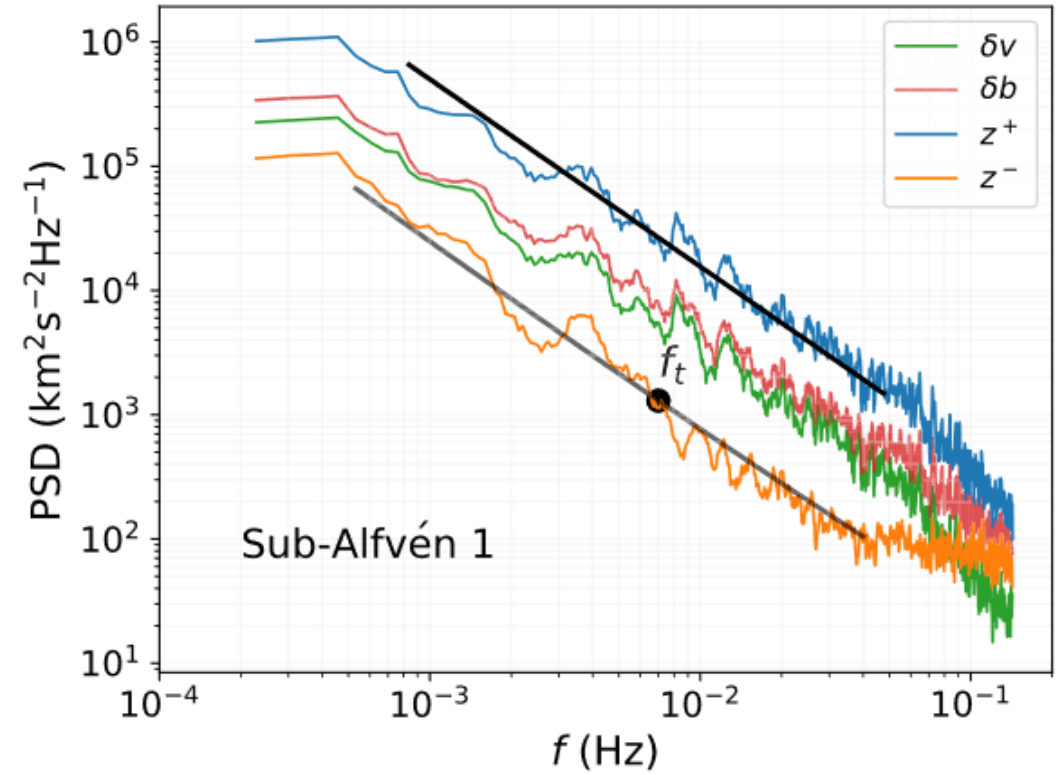
~ 0.1 AU



The Sunward mode exists, just weak compared to outward
(weaker nonlinearities)



Chen+ 2020

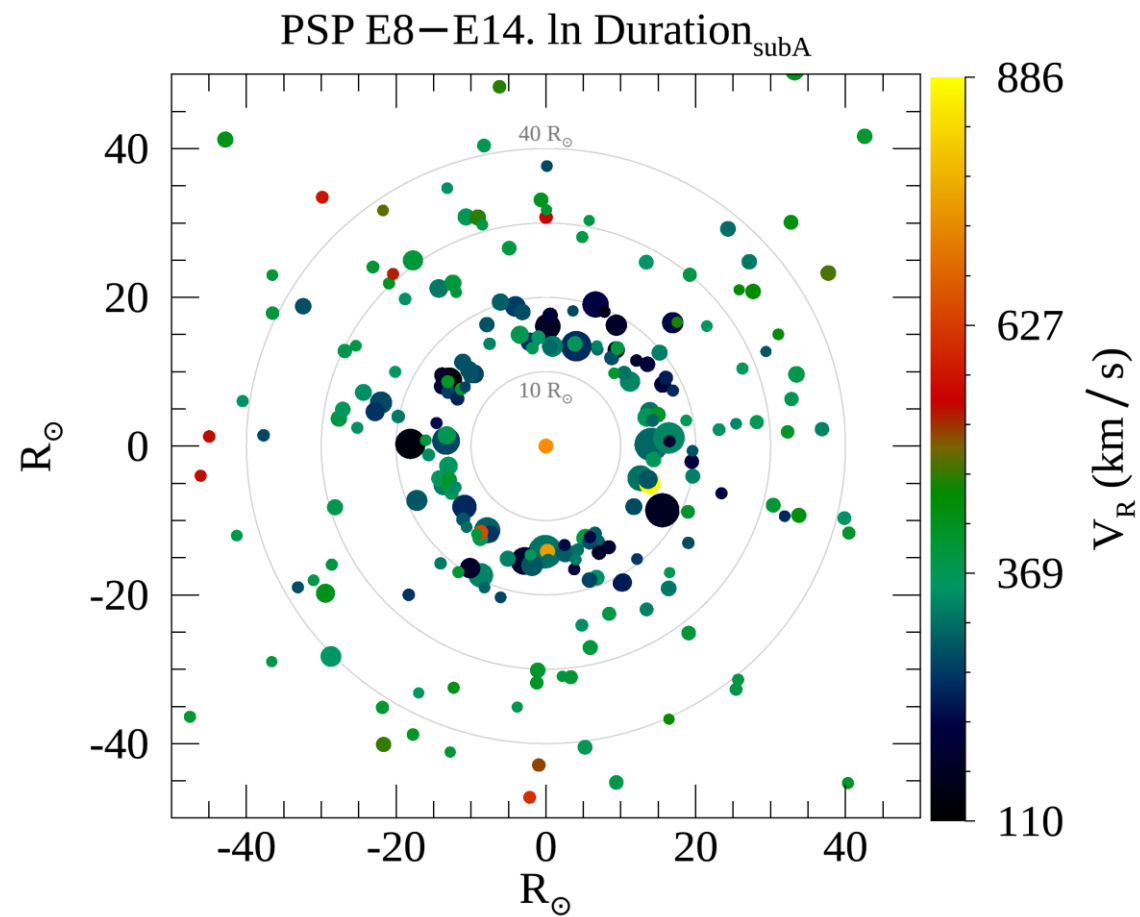
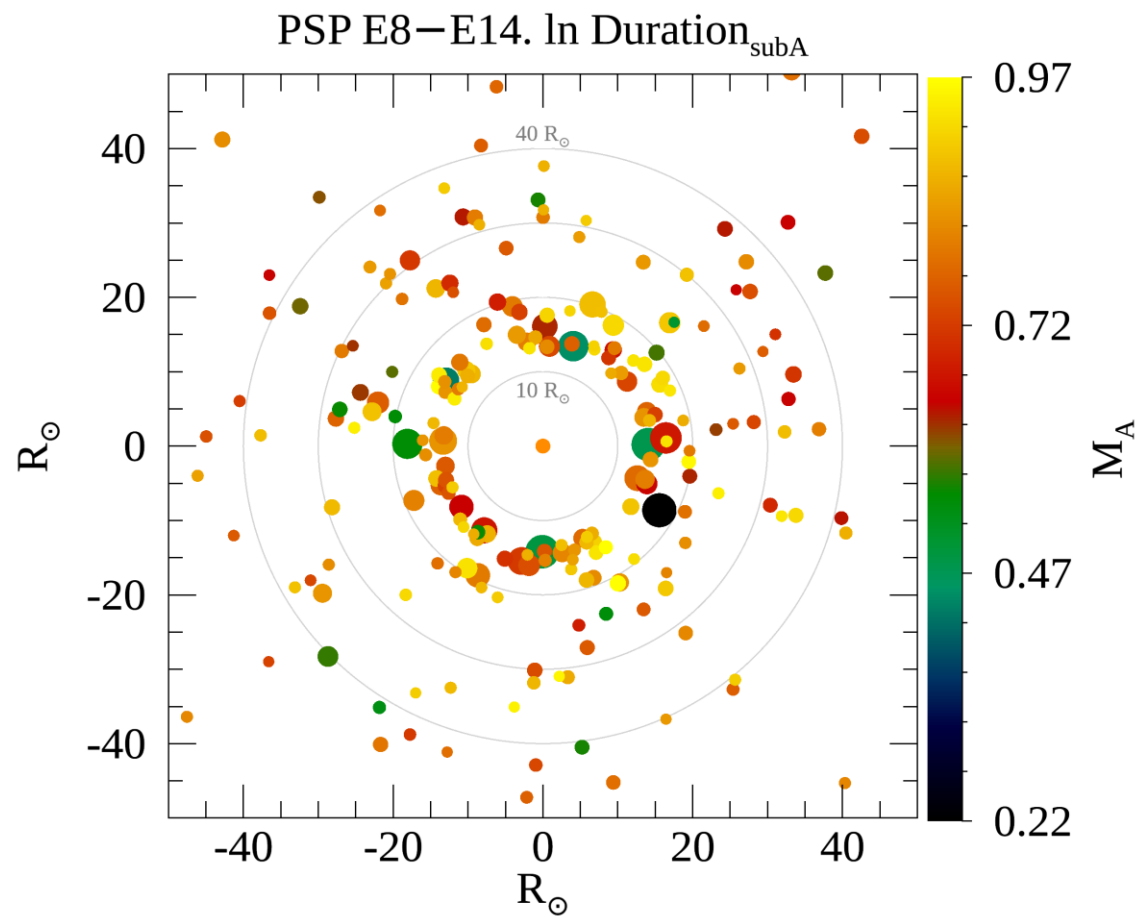


Zhao+ 2022

Conclusions

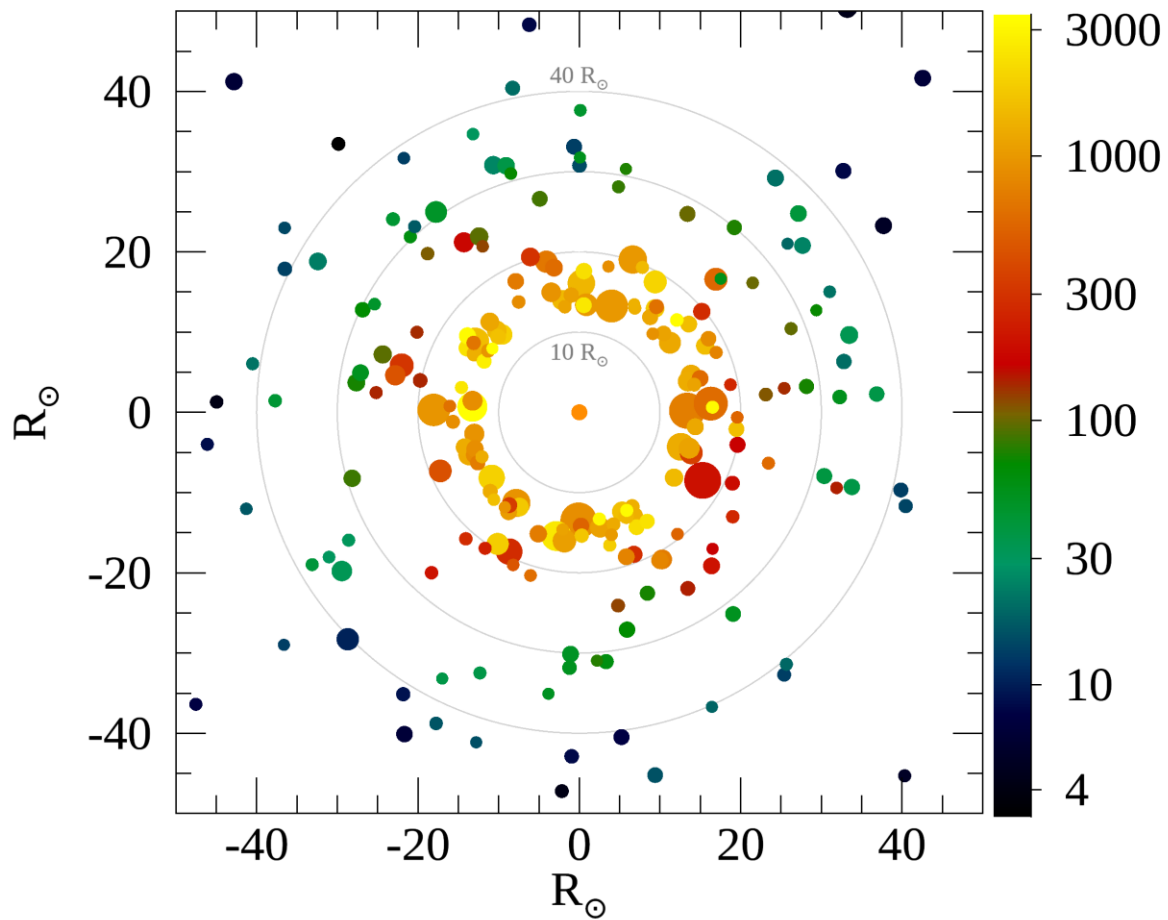
- Turbulence implies an extended spatial region of transition from subAlfvenic to superAlfvenic flow
- PSP observations consistent with patchy and fragmented morphology of Alfven zone, extending over a range of helioradii
- (Preliminary) Intervals with dominant Sunward propagation of Alfven waves are rare near Alfven surface; strength of Sunward mode continues to decrease crossing below Alfven surface: weaker NL interactions

Global properties of Alfvén zone

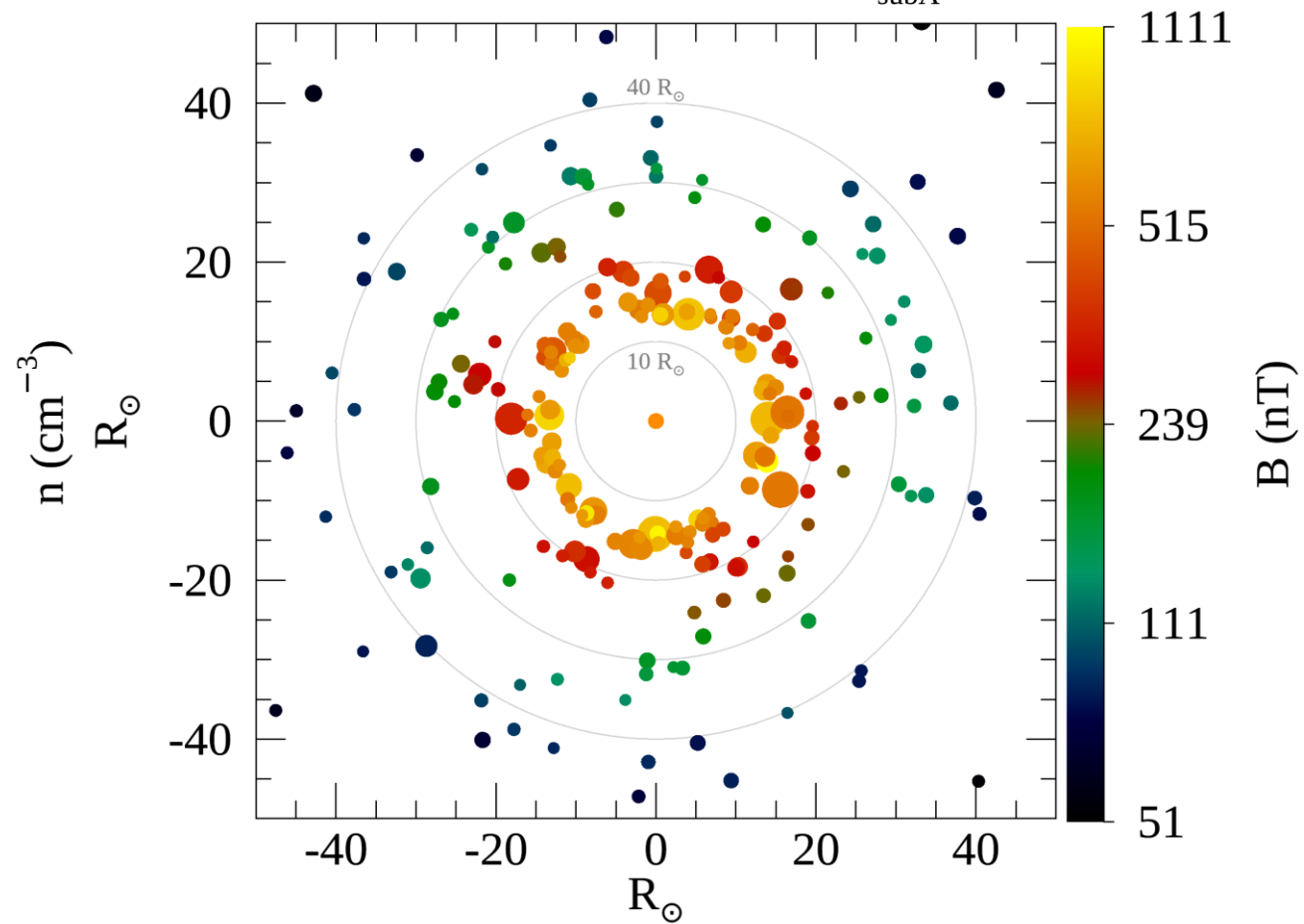


Global properties of Alfvén zone

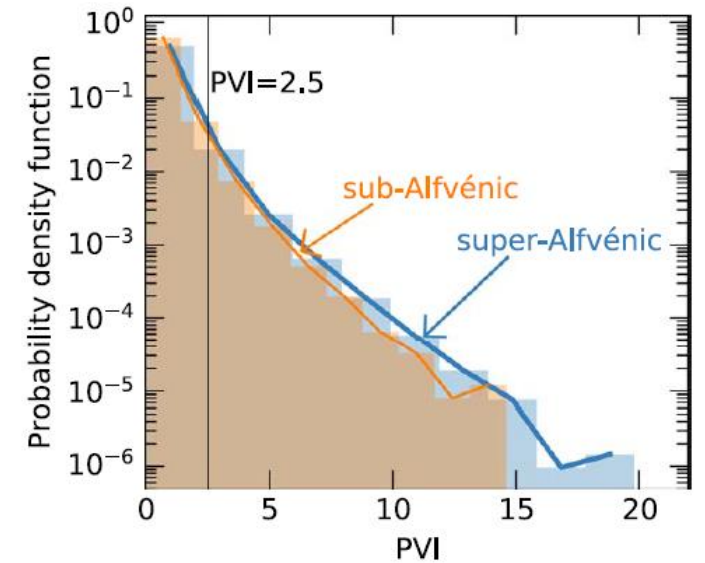
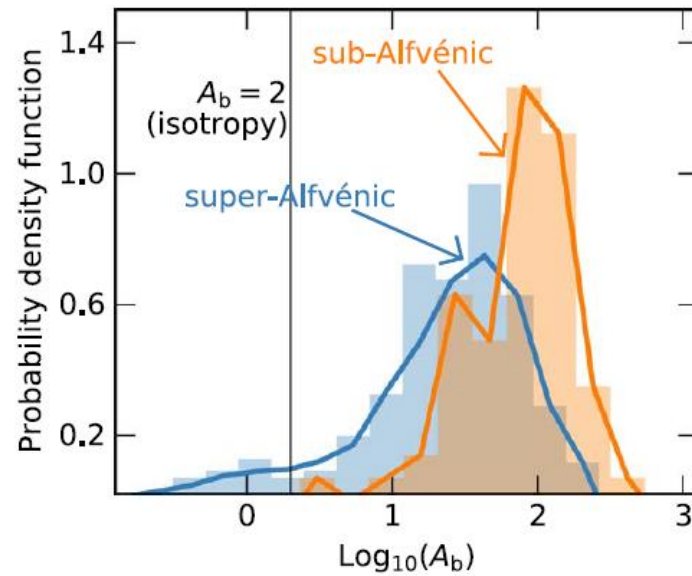
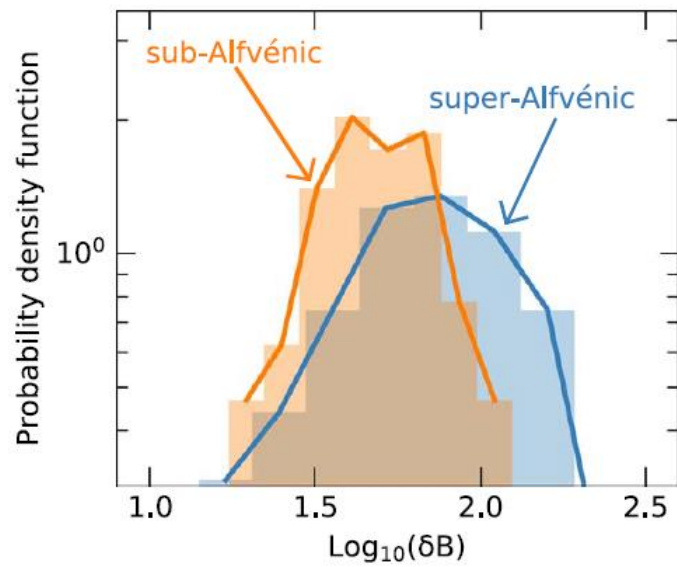
PSP E8–E14. In Duration_{subA}



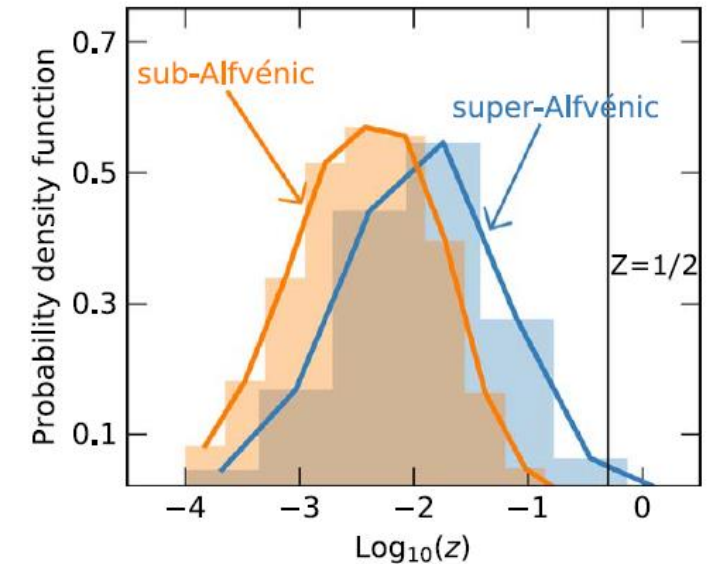
PSP E8–E14. In Duration_{subA}



Turbulence compared between subAlfvénic and superAlfvénic intervals (PSP)

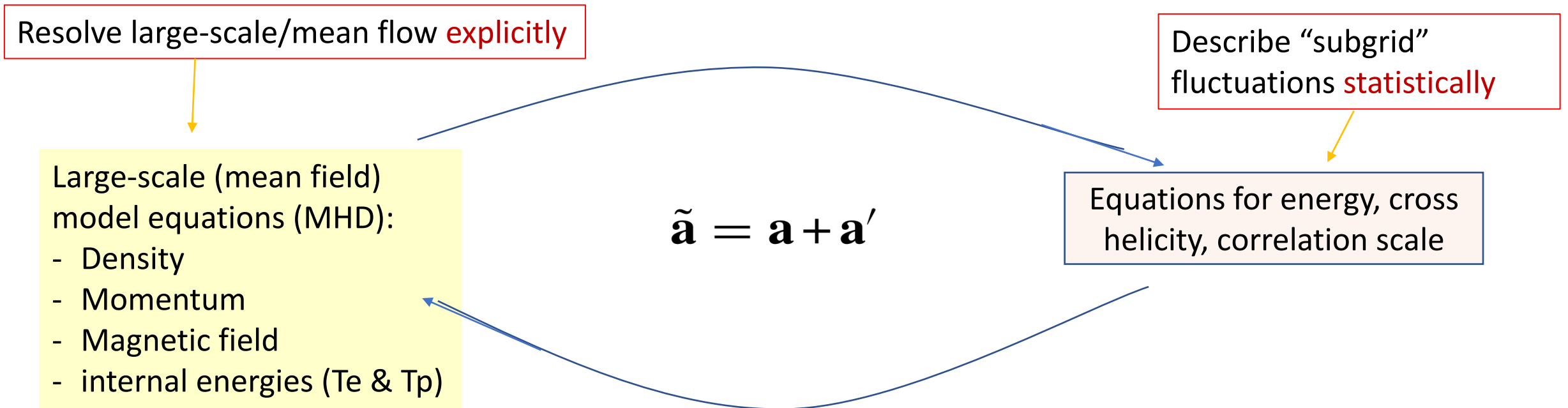


Clockwise from top left – fluctuation amplitude, variance anisotropy, intermittency (PVI), number of switchbacks



Global simulation with turbulence modeling – Schematic of Reynolds-Averaging Approach

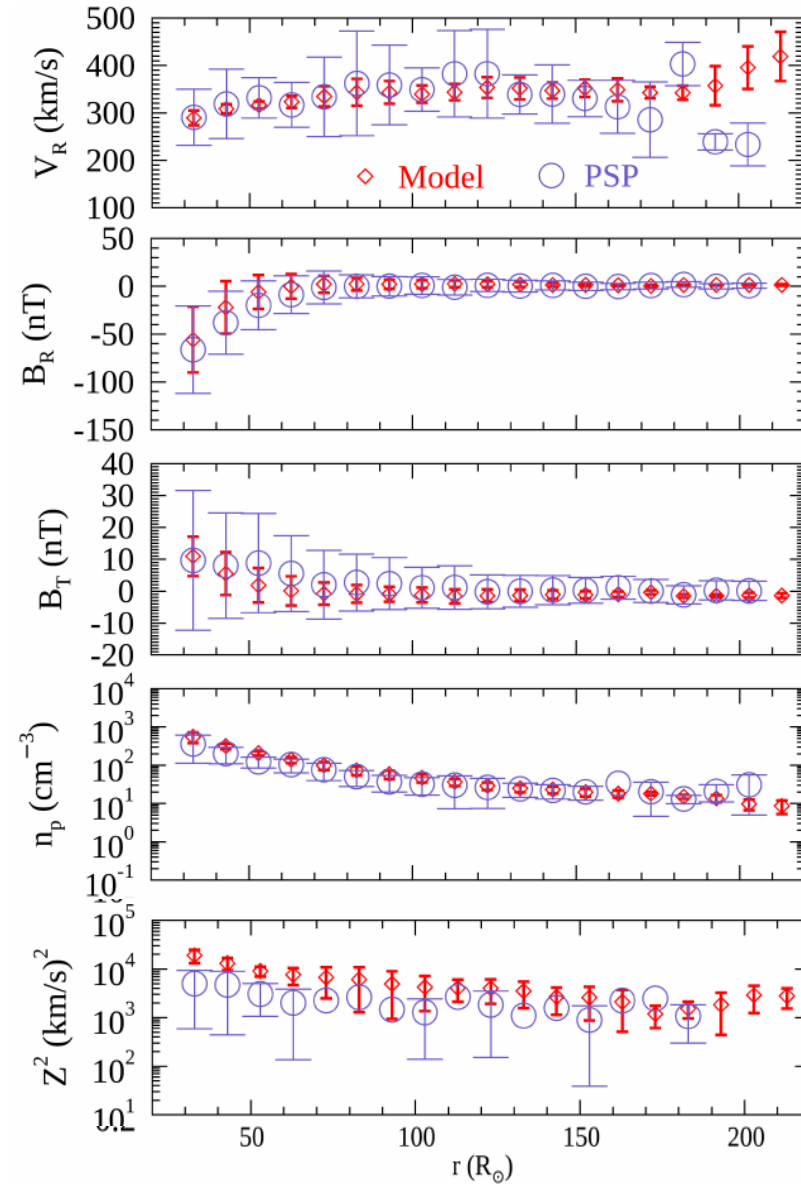
- Global simulation of corona/solar wind cannot explicitly resolve turbulence
- Reynolds decomposition splits fields ($\tilde{\mathbf{a}}$) into mean (\mathbf{a}) and fluctuation (\mathbf{a}' ; arbitrary amplitude)



- Two-way coupling – turbulence accelerates and heats wind, and gradients in large-scale fields drive turbulence
- Well-tested, good agreement with observations (Usmanov+ 2018, Chhiber+ 2021)

Global sim w' turbulence modeling – Comparison with five PSP orbits

$$Z^2 = \langle v'^2 + b'^2 \rangle$$



Two-Fluid Reynolds Averaged MHD Equations

$$\frac{\partial \rho}{\partial t} + \nabla \cdot (\rho \mathbf{v}) = 0$$

$$\frac{\partial(\rho \mathbf{u})}{\partial t} + \nabla \cdot \left[\rho \mathbf{v} \mathbf{u} - \frac{1}{4\pi} \mathbf{B} \mathbf{B} + \left(P_S + P_E + \frac{B^2}{8\pi} + \frac{\langle B'^2 \rangle}{8\pi} \right) \mathbf{I} + \mathcal{R} \right] = -\rho \left(\frac{GM_\odot}{r^2} + \boldsymbol{\Omega} \times \mathbf{u} \right)$$

$$\frac{\partial \mathbf{B}}{\partial t} = \nabla \times (\mathbf{v} \times \mathbf{B} + \boldsymbol{\varepsilon}_m \sqrt{4\pi\rho})$$

$$\frac{\partial P_S}{\partial t} + (\mathbf{v} \cdot \nabla) P_S + \gamma P_S \nabla \cdot \mathbf{u} + (\gamma - 1) \frac{P_S - P_E}{\tau_{SE}} = f_p Q_T$$

$$\frac{\partial P_E}{\partial t} + (\mathbf{v} \cdot \nabla) P_E + \gamma P_E \nabla \cdot \mathbf{u} + (\gamma - 1) \left[\frac{P_E - P_S}{\tau_{SE}} + \nabla \cdot \mathbf{q}_H \right] = (1 - f_p) Q_T$$

- P_S and P_E are the proton and electron pressure
- \mathbf{u} is the velocity in the inertial frame
- \mathbf{v} is the velocity in the rotating frame
- τ_{SE} is the electron-proton Coulomb collision rate
- $\mathcal{R} = \langle \rho \mathbf{v}' \mathbf{v}' - \frac{\mathbf{B}' \mathbf{B}'}{4\pi} \rangle$ is the Reynolds stress tensor
- $\boldsymbol{\varepsilon}_m = \frac{\langle \mathbf{v}' \times \mathbf{B}' \rangle}{(4\pi\rho)^{1/2}}$ is the mean turbulent electric field
- Q_T is the turbulent heating rate
- \mathbf{q}_H is the electron heat flux

Two-Fluid Reynolds-averaged MHD with Turbulence Transport

- Turbulence transport equations obtained by subtracting mean-flow eqns. from full eqns., and averaging.

mean flow

$$\frac{\partial \rho}{\partial t} + \nabla \cdot (\rho \mathbf{v}) = 0$$

$$\frac{\partial(\rho \mathbf{u})}{\partial t} + \nabla \cdot \left[\rho \mathbf{v} \mathbf{u} - \frac{1}{4\pi} \mathbf{B} \mathbf{B} + \left(P_S + P_E + \frac{B^2}{8\pi} + \frac{\langle B'^2 \rangle}{8\pi} \right) \mathbf{I} + \mathcal{R} \right] = -\rho \left(\frac{GM_\odot}{r^2} + \boldsymbol{\Omega} \times \mathbf{u} \right)$$

$$\frac{\partial \mathbf{B}}{\partial t} = \nabla \times (\mathbf{v} \times \mathbf{B} + \boldsymbol{\varepsilon}_m \sqrt{4\pi\rho})$$

$$\frac{\partial P_S}{\partial t} + (\mathbf{v} \cdot \nabla) P_S + \gamma P_S \nabla \cdot \mathbf{u} + (\gamma - 1) \frac{P_S - P_E}{\tau_{SE}} = f_p Q_T$$

$$\frac{\partial P_E}{\partial t} + (\mathbf{v} \cdot \nabla) P_E + \gamma P_E \nabla \cdot \mathbf{u} + (\gamma - 1) \left[\frac{P_E - P_S}{\tau_{SE}} + \nabla \cdot \mathbf{q}_H \right] = (1 - f_p) Q_T$$

- $Z^2 = \langle v'^2 + b'^2 \rangle$ is (twice the incompressible turbulent energy per unit mass)
- $\sigma_c = \frac{2\langle \mathbf{v}' \cdot \mathbf{b}' \rangle}{\langle v'^2 + b'^2 \rangle}$ is the normalized cross helicity
- λ is the similarity (correlation) length scale

Turbulence modeling assumptions –

- Incompressible and transverse fluctuations
- Turbulent stresses modeled in terms of large-scale gradients (shear)
- NL terms modeled dimensionally (von Karman similarity)

- Physically and empirically motivated ICs and BCs
- Magnetogram-based or dipolar source magnetic field
- Numerical domain from coronal base to few AU

turbulence

$$\frac{\partial Z^2}{\partial t} + (\mathbf{v} \cdot \nabla) Z^2 + \frac{(1 - \sigma_D) Z^2}{2} \nabla \cdot \mathbf{u} + \frac{2}{\rho} \mathcal{R} : \nabla \mathbf{u} + 2\boldsymbol{\varepsilon}_m \cdot (\nabla \times \mathbf{u}) - (\mathbf{V}_A \cdot \nabla)(Z^2 \sigma_c) + Z^2 \sigma_c \nabla \cdot \mathbf{V}_A = -\frac{\alpha f^+(\sigma_c) Z^3}{\lambda}$$

$$\frac{\partial(Z^2 \sigma_c)}{\partial t} + (\mathbf{v} \cdot \nabla)(Z^2 \sigma_c) + \frac{Z^2 \sigma_c}{2} \nabla \cdot \mathbf{u} + \frac{2}{\rho} \mathcal{R} : \nabla \mathbf{V}_A + 2\boldsymbol{\varepsilon}_m \cdot (\nabla \times \mathbf{u}) - (\mathbf{V}_A \cdot \nabla) Z^2 + (1 - \sigma_D) Z^2 \nabla \cdot \mathbf{V}_A = -\frac{\alpha f^-(\sigma_c) Z^3}{\lambda}$$

$$\frac{\partial \lambda}{\partial t} + (\mathbf{v} \cdot \nabla) \lambda = \beta f^+(\sigma_c) Z$$

See Usmanov et al., 2018 for more details

Closures and other terms (extra slide)

- Electron-proton collision frequency:

$$\nu_E = \frac{8(2\pi m_e)^{1/2} e^4 N_E \ln \Lambda}{3m_p (k_B T_E)^{3/2}} \quad \ln \Lambda = \ln \left[\frac{3(k_B T_E)^{3/2}}{2\pi^{1/2} e^3 N_E^{1/2}} \right]$$

- Classical (Spitzer) electron heat conduction (below $5 R_\odot$):

$$\mathbf{q}_S = -\kappa \hat{\mathbf{B}} (\hat{\mathbf{B}} \cdot \nabla) T_E \quad \kappa = 8.4 \times 10^{-7} T_E^{5/2}$$

- Collisionless (Hollweg) heat conduction: $\mathbf{q}_H = (3/2)\alpha_H P_E \mathbf{v}$

- Turbulent heating: $Q_T = \frac{\alpha f^+(\sigma_c) \rho Z^3}{2\lambda}$

- TSDIA closure for turbulent stresses:

$$\boldsymbol{\varepsilon}_m = \bar{\alpha} \mathbf{B} - \bar{\beta} \nabla \times \mathbf{V}_A + \bar{\gamma} \nabla \times \mathbf{v}$$

$$\nu_M = (7/5) \bar{\gamma}$$

$$\nu_K = (7/5) \bar{\beta}$$

$$\frac{1}{\rho} \mathcal{R} = \frac{2}{3} K_R \mathbf{I} - \nu_K \mathcal{S} + \nu_M \mathcal{M}$$

$$K_R = \sigma_D Z^2 / 2$$

$$\mathcal{S} = \nabla \mathbf{u} + \nabla \mathbf{u}^T - \frac{2}{3} (\nabla \cdot \mathbf{u}) \mathbf{I}$$

$$\mathcal{M} = \nabla \mathbf{V}_A + \nabla \mathbf{V}_A^T - \frac{2}{3} (\nabla \cdot \mathbf{V}_A) \mathbf{I}$$

$$\nu_K \approx 0.27 Z \lambda \quad \nu_M \approx 0.22 \sigma_c Z \lambda$$

Modeling NL terms

$$\frac{\partial \mathbf{z}_\pm}{\partial t} = -\mathbf{z}_\mp \cdot \nabla \mathbf{z}_\pm$$

$$\frac{\partial}{\partial t} \langle z_+^2 \rangle = -2 \langle \mathbf{z}_+ \cdot (\mathbf{z}_- \cdot \nabla \mathbf{z}_+) \rangle$$

$$\sim -\langle z_+^2 \rangle \frac{\langle z_-^2 \rangle^{-1/2}}{\lambda_+},$$

$$\frac{\partial Z^2}{\partial t} \sim -\frac{Z^3}{\lambda}$$

Boundary/Initial conditions and parameters (extra slide)

| Symbol | Description | Value |
|---------------|---|---------------------------------|
| N_0 | proton number density in the initial state at $1 R_\odot$ | $8 \times 10^7 \text{ cm}^{-3}$ |
| T_0 | electron and proton temperature in the initial state at $1 R_\odot$ | $1.8 \times 10^6 \text{ K}$ |
| B_0 | magnetic field strength of dipole at $1 R_\odot$ | 12 G |
| δv_0 | driving amplitude of fluctuations in the initial state at $1 R_\odot$ | 35 km s^{-1} |
| σ_{e0} | normalized cross helicity in the initial state | 0.8 |
| λ_0 | correlation scale of turbulence in the initial state at $1 R_\odot$ | $0.015 R_\odot$ |

| Symbol | Description | Value |
|-----------------|--|-------------|
| σ_D | normalized energy difference (residual energy) | $-1/3$ |
| γ | adiabatic index | $5/3$ |
| α_H | constant in Hollweg's collisionless heat flux | 1.05 |
| α, β | Kármán–Taylor constants | 2, 0.128 |
| f_p | fraction of turbulent heating for protons | 0.6 |
| r_H | collisional/collisionless electron heat flux transition region | $5 R_\odot$ |

Spatial Scales Resolved in Simulations

- Resolution $\sim 700 \times 120 \times 240$ in r, θ, ϕ ($r = 1 R_{\odot} - 5 \text{ AU}$)
- Grid scale Δ is generally within a factor of few correlation scales

